

# Training Uncertainty-Aware Classifiers with Conformalized Deep Learning

Bat-Sheva Einbinder<sup>\*1</sup>Yaniv Romano<sup>12</sup>Matteo Sesia<sup>3</sup>Yanfei Zhou<sup>3</sup>

## Abstract

Deep neural networks are powerful tools to detect hidden patterns in data and leverage them to make predictions, but they are not designed to understand uncertainty and estimate reliable probabilities. In particular, they tend to be overconfident. We begin to address this problem in the context of multi-class classification by developing a novel training algorithm producing models with more dependable uncertainty estimates, without sacrificing predictive power. The idea is to mitigate overconfidence by minimizing a loss function, inspired by advances in conformal inference, that quantifies model uncertainty by carefully leveraging hold-out data. Experiments with synthetic and real data demonstrate this method can lead to smaller conformal prediction sets with higher conditional coverage, after exact calibration with hold-out data, compared to state-of-the-art alternatives.

## 1 Introduction

The predictions of deep neural networks and other complex machine learning (ML) models affect important decisions in many applications [1–6], including autonomous driving, medical diagnostics, or security monitoring. Prediction errors in those contexts can be costly or even dangerous, which makes dependable and explainable uncertainty estimation essential. Unfortunately, deep neural networks are not designed to understand uncertainty and they are easily prone to overfitting; consequently, they may lead to overconfidence [7–9]. Overconfidence is especially problematic in the face of *aleatory* uncertainty [10], which refers to situations in which the outcome to be predicted is intrinsically noisy. Unlike the complementary *epistemic* uncertainty, aleatory uncertainty cannot be eliminated by training a more flexible model or by increasing the sample size. For example, think of prognosticating COVID-19 survival [11, 12], assessing genetic disease predisposition [13–15], or anticipating credit card defaults [16]. In those applications, the outcome of interest is potentially complicated and likely depends on many unmeasured variables. Therefore, no practical model may achieve perfect accuracy, but models that can offer practitioners principled measures of confidence for each individual-level prediction naturally tend to be more useful and trustworthy. Among many existing techniques for estimating uncertainty in ML predictions [7–9], conformal inference [17], stands out for its ability to provide finite-sample guarantees without unrealistic algorithmic simplifications and without strong assumptions about the data generating process or the underlying sources of uncertainty.

Conformal inference is designed to convert the output of any ML model into a *prediction set* of likely outcomes whose size is automatically tuned using *hold-out data*, in such a way that the same procedure applied to future test data will yield prediction sets that are well calibrated in a frequentist sense. In particular, these sets have provable *marginal coverage*; i.e., at the 90% level this means the outcome for a new random test point is contained in the output set 90% of the time. The hold-out

<sup>\*</sup>Authors listed in alphabetical order.

<sup>1</sup>Department of Electrical and Computer Engineering, Technion, Israel.

<sup>2</sup>Department Computer Science, Technion, Israel.

<sup>3</sup>Department of Data Sciences and Operations, University of Southern California, Los Angeles, CA, USA.

data are utilized to evaluate *conformity scores*, or goodness-of-fit scores, whose ordering determines how the sets are to be expanded so that the desired fraction of test points is guaranteed to be covered.

A limitation of conformal inference is that it involves of two distinct phases, training and calibration, that are generally not designed to work together efficiently. The calibration algorithm takes as input pre-trained models that may already be overconfident, and this is sub-optimal because bad habits are harder to correct after they become entrenched. As a result of this uncoordinated two-step approach, conformal predictions may be either unnecessarily conservative or overconfident for certain types of test cases, which can make them unreliable [18, 19] and unfair [20]. We address this challenge by developing a new ML training method that synergetically combines the learning and calibration phases of conformal inference, reducing the overconfidence of the predictions calculated by the output model. The idea is to minimize a new loss function designed to measure the discrepancy in distribution between the conformity scores computed by the current model estimate and those of an imaginary oracle that can leverage perfect knowledge of the data generating process to construct the most informative and reliable possible predictions. As we will demonstrate empirically, applying standard conformal inference (based on independent calibration data) to models trained with our novel algorithm leads to smaller prediction sets with more accurate coverage for all test points. In other words, the “uncertainty-aware” ML models trained with the proposed algorithm tend to work more efficiently within a standard conformal inference framework compared to black-box models, which perhaps should not be surprising. Further, we will also show that the models obtained with our method produce relatively reliable prediction sets even if the post-training conformal calibration step is omitted, although the latter remains necessary in theory to guarantee valid coverage.

## Related work

Many methods have been developed to mitigate overconfidence in ML [21–34], for example by allowing an *agnostic* output, by suitable post-processing [7, 35–40], or through early stopping [41]. Additional relevant research includes that of [42–46, 46–52], and these will provide us with informative benchmarks. However, unlike conformal inference, these methods have no frequentist guarantees in finite samples, and largely rely on loss functions targeting the accuracy of best-guess predictions, without explicitly addressing uncertainty during training. We build upon conformal inference [53–58], pioneered by [17], which typically deals with off-the-shelf models [17, 19, 59, 60]. Although other very recent works have proposed leveraging ideas from this field to improve training [61–66], this paper is novel as it combines the adaptive conformity scores of [19] with a completely new uncertainty-aware loss function. This departs from [62, 63], which sought to minimize the cardinality of the prediction sets, and from [61, 64–66], which utilized conformal inference ideas for tuning low-dimensional hyper-parameters as opposed to fully guiding the training of all model parameters. Although we focus on classification [19], our method could be repurposed for regression [58, 67] and other supervised tasks [60, 68, 69]. Conformal inference can also be utilized to test hypotheses and calibrate probabilities [70], and our work could be extended to those problems.

## 2 Relevant background on conformal inference

### 2.1 Uncertainty quantification via conformal prediction sets

Consider a data set of i.i.d. (or sometimes simply *exchangeable*) observations  $(X_i, Y_i)_{i=1}^{n+1}$  sampled from an arbitrary unknown distribution  $P_{XY}$ . Here,  $X_i \in \mathbb{R}^p$  contains  $p$  features for the  $i$ th sample, and  $Y_i \in \{1, \dots, K\} = [K]$  denotes its label, which we assume to be one of  $K$  possible categories. The goal is to train a model on  $n$  data points,  $(X_i, Y_i)_{i=1}^n$ , and construct a reasonably small prediction set  $\hat{C}_{n,\alpha} \subseteq [K]$  for  $Y_{n+1}$  given  $X_{n+1}$  such that, for some fixed level  $\alpha \in (0, 1)$ ,

$$\mathbb{P} \left[ Y_{n+1} \in \hat{C}_{n,\alpha}(X_{n+1}) \right] \geq 1 - \alpha. \quad (1)$$

This property is called *marginal coverage* because it treats  $(X_i, Y_i)_{i=1}^{n+1}$  as all random. If  $\alpha = 0.1$ , it ensures  $Y_{n+1}$  is contained in the prediction sets 90% of the time. Marginal coverage is practically feasible but not fully satisfactory, as it is not as reliable and informative as *conditional coverage*:

$$\mathbb{P} \left[ Y_{n+1} \in \hat{C}_{n,\alpha}(x) \mid X_{n+1} = x \right] \geq 1 - \alpha, \quad \forall x \in \mathbb{R}^p. \quad (2)$$

Conditional coverage would give one confidence that  $\hat{C}_{n,\alpha}(x)$  contains the true  $Y$  for any individual data point, which is stronger than (1). For example, imagine a population in which color is a feature and 90% of samples are blue while the others are red. Then, 90% marginal coverage is attained by any prediction sets that contain the true  $Y$  for all blue samples but never do for the red ones. Valid coverage can be obtained conditional on a given *protected category* [20], but it is impossible to guarantee (2) more generally without unrealistically strong assumptions [71, 72]. Thus, a typical compromise is to construct prediction sets with marginal coverage and hope they are also reasonably valid conditional on  $X$ . For multi-class classification, a solution is offered by the conformity scores developed in [19], which are reviewed below as the starting point of our contribution.

## 2.2 Review of adaptive conformity scores for classification

Imagine an *oracle* knowing the conditional distribution of  $Y$  given  $X$ , namely  $P_{Y|X}$ , and think of how it would construct the smallest possible prediction sets  $C_\alpha^{\text{oracle}}(x)$  with exact  $1 - \alpha$  conditional coverage. For any  $x \in \mathcal{X}$  and  $y \in [K]$ , define  $\pi_y(x) = \mathbb{P}[Y = y \mid X = x]$ . Then, the oracle would output the smallest subset  $S \subseteq [K]$  such that  $\sum_{y \in S} \pi_y(x) \geq 1 - \alpha$ . In truth, this set may have coverage strictly larger than  $1 - \alpha$  due to the discreteness of  $Y$ ; however, exact coverage can be achieved by introducing a little extra randomness [20]. For any nominal coverage level  $\tau \in (0, 1)$  and any random noise variable  $u \in (0, 1)$ , let  $\mathcal{S}$  be the function with input  $x, u, \pi$ , and  $\tau$  that computes the set of most likely labels up to (but possibly excluding) the one identified by the above deterministic oracle:  $\mathcal{S}(x, u; \pi, \tau) \subseteq [K]$ . Note that the explicit expression of  $\mathcal{S}$  is written in Appendix A1.1. If  $u = U$  is a uniform random variable independent of everything else, it is easy to verify that the following oracle prediction sets have exact conditional coverage at level  $\tau = 1 - \alpha$ :

$$C_\alpha^{\text{oracle}}(x) = \mathcal{S}(x, U; \pi, 1 - \alpha). \quad (3)$$

For example, if  $\pi_1(x) = 0.3$ ,  $\pi_2(x) = 0.6$ , and  $\pi_3(x) = 0.1$ , then  $C_{0.2}^{\text{oracle}}(x) = \{1, 2\}$  with probability  $2/3$ , and  $C_{0.2}^{\text{oracle}}(x) = \{2\}$  with probability  $1/3$ . Of course, this oracle is only a thought experiment because  $P_{Y|X}$  is generally unknown. Therefore, to construct practical prediction intervals,  $\pi$  must be replaced by an ML model  $\hat{\pi}$ . Then, conformal inference is needed to ensure the output sets based on the possibly inaccurate ML model at least satisfy marginal coverage (1).

Conformal inference [19] begins by training any classifier on part of the data, indexed by  $\mathcal{D}_1 \subset [n]$ , to fit an approximation  $\hat{\pi}$  of the unknown  $\pi$ . After substituting  $\hat{\pi}$  into the oracle rule  $\mathcal{S}$ , the hold-out data indexed by  $\mathcal{D}_2 = [n] \setminus \mathcal{D}_1$  are leveraged to adjust the prediction sets as to empirically achieve the desired coverage. More precisely, define the following *conformity scores*  $W_i$  for all observations in  $\mathcal{D}_2$ , and for the test point  $n + 1$ . Intuitively,  $W_i$  is the smallest  $\tau \in [0, 1]$  such that  $\mathcal{S}(X_i, U_i; \hat{\pi}, \tau)$  contains the true  $Y_i$ , while  $U_i$  is a uniform random variable independent of everything else:

$$W_i = W(X_i, Y_i, U_i; \hat{\pi}) = \min \{ \tau \in [0, 1] : Y_i \in \mathcal{S}(X_i, U_i; \hat{\pi}, \tau) \}, \quad i \in \mathcal{D}_2 \cup \{n + 1\}. \quad (4)$$

These statistics are observed for all  $i \in \mathcal{D}_2$ , but not for  $n + 1$ . Define also  $\hat{\tau}_{n,\alpha}$  as the  $\lceil (1 - \alpha)(1 + |\mathcal{D}_2|) \rceil$  largest element of  $\{W_i\}_{i \in \mathcal{D}_2}$ . Intuitively,  $\hat{\tau}_{n,\alpha}$  is the smallest  $\tau \in [0, 1]$  such that  $\mathcal{S}(X_i; \hat{\pi}, \tau)$  contains a fraction  $1 - \alpha$  of the hold-out data in  $\mathcal{D}_2$ . Then, the output prediction set for a new  $X_{n+1}$  is  $C_{n,\alpha}(X_{n+1}) = \mathcal{S}(X_{n+1}, U_{n+1}; \hat{\pi}, \hat{\tau}_{n,\alpha})$ . This has  $1 - \alpha$  marginal coverage due to the exchangeability of the calibration and test data [19]. In fact,  $Y_{n+1} \notin C_{n,\alpha}(X_{n+1})$  implies  $W_{n+1} > \hat{\tau}_{n,\alpha}$ , and by exchangeability the probability of this event is smaller than  $\alpha$ ; see [58]. Unlike alternative approaches based on different scores [17, 18, 53], this solution would yield prediction sets equivalent to those of the oracle [19] if  $\hat{\pi} = \pi$ . Although generally  $\hat{\pi} \neq \pi$ , the above prediction sets often achieve relatively high conditional coverage [19] in practice. Our goal is to further improve their empirical performance by training the ML model to be more deliberately aware of uncertainty.

## 3 Methods

### 3.1 The distribution of the adaptive conformity scores

The conformity scores defined in (4) are uniformly distributed conditional on  $X = x$ , for any  $x$ , if  $\hat{\pi} = \pi$ . This property was hinted without proof in [19] and it serves as the starting point of our contribution. Note that all mathematical proofs can be found in Appendix A2.

**Proposition 1.** *The distribution of the conformity scores  $W_i$  in (4) is uniform conditional on  $X_i$  if  $\hat{\pi} = \pi$ . That is,  $\mathbb{P}[W(X, Y, U; \pi) \leq \beta \mid X = x] = \beta$  for all  $\beta \in (0, 1)$ , where  $(X, Y)$  is a random*

sample from  $P_{X,Y}$ , and  $U \sim \text{Uniform}[0, 1]$  independent of everything else. Further,  $W_i \mid X_i$  is uniform if and only if  $\mathcal{S}(X_i; \hat{\pi}, 1 - \alpha)$  has conditional coverage at level  $1 - \alpha$  for all  $\alpha \in [0, 1]$ .

As we seek accurate conditional coverage, this result suggests training  $\hat{\pi}$  as to produce scores that are approximately uniform on hold-out data, at least marginally. Therefore, we will evaluate (4) on hold-out data *while training*  $\hat{\pi}$ , encouraging the conformity scores to follow a uniform distribution.

### 3.2 An uncertainty-aware conformal loss function

We develop a loss function that approximately measures the deviation from uniformity of the conformity scores defined in (4) by combining classical non-parametric tests for equality in distribution with fast algorithms for smooth sorting and ranking [73, 74]. This loss is combined with the traditional cross entropy as to also promote accurate predictions, and it can be approximately optimized by stochastic gradient descent (it will generally be non-convex). The novel uncertainty-aware component of this loss only sees the hold-out samples through the lens of a non-parametric test applied to the empirical score distribution within a subset of the data. Therefore, it provides little incentive to overfit compared to a traditional loss targeting point-wise predictive accuracy, such as the cross entropy. By contrast, it discourages overconfident predictions which would yield non-uniform scores, as we shall see below. This solution is outlined in Figure A4, Appendix A1.2, and detailed below.

First, the  $n$  training samples are partitioned into two subsets,  $\mathcal{I}_1$  and  $\mathcal{I}_2$  such that  $\mathcal{I}_1 \cup \mathcal{I}_2 = [n] = \mathcal{D}_1$ . Here we assume the training data are indexed by  $\mathcal{D}_1 = [n]$ ; this notation is slightly different from Section 2, but it is simple and does not introduce ambiguity because the additional calibration data in  $\mathcal{D}_2$  remain untouched during training. The training algorithm approximately minimizes a loss function  $\ell$  consisting of two additive components, each evaluated on one subset of the data:

$$\ell = (1 - \lambda) \cdot \ell_a(\mathcal{I}_1) + \lambda \cdot \ell_u(\mathcal{I}_2). \quad (5)$$

Above, the hyper-parameter  $\lambda \in [0, 1]$  controls the relative weights of the two components. The  $\ell_a$  component is evaluated on the data in  $\mathcal{I}_1$ , and its purpose is to seek high predictive accuracy, as customary. For example, this could be the cross entropy:

$$\ell_a = -\frac{1}{|\mathcal{I}_1|} \sum_{i \in \mathcal{I}_1} \sum_{c=1}^K \mathbb{1}[Y_i = c] \log \hat{\pi}_c(X_i), \quad (6)$$

where  $\hat{\pi}$  is the output of the final softmax layer. The novel uncertainty-aware component  $\ell_u$  is evaluated on  $\mathcal{I}_2$ , and its role is to mitigate overconfidence. Concretely, conformity scores  $W_i$  are evaluated according to (4) for all  $i \in \mathcal{I}_2$ , and their empirical distribution is compared to the ideal uniformity expected if  $\hat{\pi} = \pi$ . Ideally, we would like to quantify this discrepancy by directly applying a powerful non-parametric test, for example by computing the Cramér-von Mises [75, 76] or Kolmogorov-Smirnov [77, 78] test statistics. Concretely, in the latter case,

$$\ell_u = \sup_{w \in [0, 1]} \left| \hat{F}_{|\mathcal{I}_2|}(w) - w \right|, \quad (7)$$

where  $\hat{F}_{|\mathcal{I}_2|}(\cdot)$  is the empirical cumulative distribution function (CDF) of  $W_i$  for  $i \in \mathcal{I}_2$ :  $\hat{F}_{|\mathcal{I}_2|}(w) = (1/|\mathcal{I}_2|) \sum_{i \in \mathcal{I}_2} \mathbb{1}[W_i \leq w]$ . Unfortunately,  $\hat{F}_{|\mathcal{I}_2|}(\cdot)$  is not differentiable, which makes the overall loss intractable to minimize. This requires introducing some approximations in  $\ell_u$ , as explained next.

### 3.3 Differentiable approximations

The empirical CDF of the conformity scores is not differentiable because it involves sorting, which is a non-smooth operation. Further, these scores themselves are not differentiable in the model parameters  $\theta$  because they involve ranking and sorting the estimated class probabilities  $\hat{\pi}$ . In fact, the score (4) can be computed in a closed form,

$$W_i = \hat{\pi}_{(1)}(X_i) + \hat{\pi}_{(2)}(X_i) + \dots + \hat{\pi}_{(r(Y_i, \hat{\pi}(X_i)))}(X_i) - U_i \cdot \hat{\pi}_{(r(Y_i, \hat{\pi}(X_i)))}(X_i), \quad (8)$$

where  $U_i$  is a uniform random variable independent of everything else; see Appendix A1.1 for details. Fortunately, there exist fast approximate algorithms for differentiable sorting and ranking that work well in combination with standard back-propagation [73, 74]. Note that evaluating  $W_i$  in (8)

requires accessing elements of  $(\hat{\pi}_{(1)}(X_i), \dots, \hat{\pi}_{(K)}(X_i))$  through a  $\theta$ -dependent index,  $r(Y_i, \hat{\pi}(X_i))$ , which is also non-differentiable. Therefore, indexing by  $r(Y_i, \hat{\pi}(X_i))$  must be approximated with a smooth linear interpolation; see Appendix A1.2 for further details. In conclusion, the  $\ell_u$  loss in (7) is approximated by evaluating a differentiable version of the scores in (4) as described above, and then by replacing their empirical CDF with a differentiable approximation obtained with the same techniques from [74]. This procedure, combined with stochastic gradient descent for fitting the model parameters  $\theta$ , is summarized in Algorithm 1. Although here we assume  $\mathcal{I}_1 = \mathcal{I}_2$  for simplicity, this algorithm can easily accommodate  $\mathcal{I}_1 \neq \mathcal{I}_2$ . A more technically detailed version of Algorithm 1 is provided in Appendix A1.2, and an open-source software implementation of this method is available online at <https://github.com/bat-sheva/conformal-learning>.

---

**Algorithm 1:** Conformalized uncertainty-aware training of deep multi-class classifiers

---

**Input:** Data  $\{X_i, Y_i\}_{i=1}^n$ ; hyper-parameter  $\lambda \in [0, 1]$ , learning rate  $\gamma > 0$ , batch size  $M$ ;

Randomly initialize the model parameters  $\theta^{(0)}$ ;

Randomly split the data into two disjoint subsets,  $\mathcal{I}_1, \mathcal{I}_2$ , such that  $\mathcal{I}_1 \cup \mathcal{I}_2 = [n]$ ;

Set the number of batches to  $B = (n/2)/M$  (assuming for simplicity that  $|\mathcal{I}_1| = |\mathcal{I}_2|$ );

**for**  $t = 1, \dots, T$  **do**

    Randomly divide  $\mathcal{I}_1$  and  $\mathcal{I}_2$  into  $B$  batches;

**for**  $b = 1, \dots, B$  **do**

        Evaluate (softmax) conditional probabilities  $\hat{\pi}(X_i)$  for all  $i$  in batch  $b$  of  $\mathcal{I}_1 \cup \mathcal{I}_2$ ;

        Generate a uniform independent random variable  $U_i$  for all  $i$  in batch  $b$  of  $\mathcal{I}_2$ ;

        Evaluate  $\tilde{W}_i$  for all  $i$  in batch  $b$  of  $\mathcal{I}_2$ , using  $U_i$  and a differentiable approximation of (4);

        Evaluate the gradient  $\nabla \ell_a(\theta^{(t)})$  of  $\ell_a$  in (6) using the data in batch  $b$  of  $\mathcal{I}_1$ ;

        Evaluate the gradient  $\nabla \tilde{\ell}_u(\theta^{(t)})$  of a differentiable approximation  $\tilde{\ell}_u$  of  $\ell_u$  in (7) using the differentiable scores  $\tilde{W}_i$  in batch  $b$  of  $\mathcal{I}_2$ ;

        Define  $\nabla \tilde{\ell}(\theta^{(t)}) = (1 - \lambda) \cdot \nabla \ell_a(\theta^{(t)}) + \lambda \cdot \nabla \tilde{\ell}_u(\theta^{(t)})$  based on (5);

        Update the model parameters:  $\theta^{(t)} \leftarrow \theta^{(t-1)} - \gamma \nabla \tilde{\ell}(\theta^{(t-1)})$ .

**end**

**end**

**Output:** The model  $\hat{\pi}$  corresponding to the fitted parameters  $\theta^{(T)}$ .

---

### 3.4 Theoretical analysis

The uncertainty-aware loss function in Algorithm 1 can be justified theoretically by noting that it is approximately minimized (although possibly non-uniquely) by the imaginary oracle model  $\pi$ , which yields the smallest possible prediction sets with exact conditional coverage. This analysis focuses on the original version of the loss function defined in (5)–(7), ignoring for simplicity the additional subtleties introduced by the differentiable approximations described in Section 3.3.

**Proposition 2.** *The loss function  $\ell \geq 0$  in (5) is bound from above by  $\ell^0 + \delta\ell$ , where  $\ell^0 \geq 0$  attains value zero if  $\hat{\pi} = \pi$ , and  $\delta\ell = \mathcal{O}_{\mathbb{P}}(1/\sqrt{M})$  as  $\mathcal{I}_2 \rightarrow \infty$ .*

Of course, Algorithm 1 does not minimize (5) exactly because it involves solving a high-dimensional non-convex optimization problem that is difficult to study theoretically. Yet, it is possible to prove at least a weak form of convergence for its stochastic gradient descent, whose solution may not however necessarily approach a global minimum. This analysis is in Appendix A2 for lack of space.

## 4 Numerical experiments

### 4.1 Experiments with synthetic data

The performance of Algorithm 1 is investigated here on synthetic data that mimic a multi-class classification problem in which most samples are relatively easy to classify but a few are unpredictable. Specifically, data are simulated with 100 independent and uniformly distributed features  $X = (X_1, \dots, X_{100}) \in [0, 1]^{100}$  and a label  $Y \in [K]$ , for  $K = 6$ . The first feature controls whether the sample is intrinsically difficult to classify, while the next two features determine the most likely

labels; all other features are useless. On average, 20% of the samples are impossible to classify with absolute confidence. This conditional distribution is written explicitly in Appendix A3.1.

The conditional class probabilities  $\hat{\pi}$  are estimated as the output of a final softmax layer in a fully connected neural network implemented with PyTorch [79]; see Appendix A3.1 for more information about network architecture and training details. This model is fitted separately with Algorithm 1 and three benchmark techniques including traditional cross entropy minimization and focal loss minimization [80]. Unfortunately, we cannot directly compare to the recent methods of [62, 63] as originally implemented by those authors for lack of openly available computer code. Instead, we consider a hybrid benchmark that combines elements of Algorithm 1 with the main idea of [63], essentially seeking a model that yields small conformal prediction sets, irrespective of conditional coverage; see Appendix A1.3 for details about this benchmark. As early stopping can help mitigate overfitting [41], it is informative to also investigate its effect on each of the aforementioned learning algorithms. For this purpose, we generate an additional validation set of 2000 independent data points and use it to preview the out-of-sample accuracy and loss value at each epoch. Then, the best versions of each model according to these two early stopping criteria are saved during training. After training each model, 10,000 additional independent samples are utilized to calibrate split-conformal prediction sets with 90% marginal coverage, as explained in Section 2.2. All models, including those trained with our method, undergo conformal calibration with these independent data points prior to constructing the prediction sets, as this step is necessary to theoretically guarantee marginal coverage. Further, we ensure the comparisons between different models are always fair by giving each training algorithm access to exactly the same data set, regardless of whether its inner workings involve sample splitting to evaluate separately distinct components of the loss function.

Figure 1 compares the performance of conformal prediction sets obtained with each model for 2000 test points as a function of the number of training samples, averaging over 50 independent experiments. The prediction sets are evaluated in terms of their average size and coverage conditional on  $X_1 \leq \delta$ ; i.e., separately for the “hard” samples. For each learning algorithm, the results corresponding to the model achieving the highest conditional coverage among the fully trained and two early stopped alternatives are reported. This allows us to focus on the overall behaviour of different losses while accounting for possible differences in the optimal choices of early-stopping strategies.

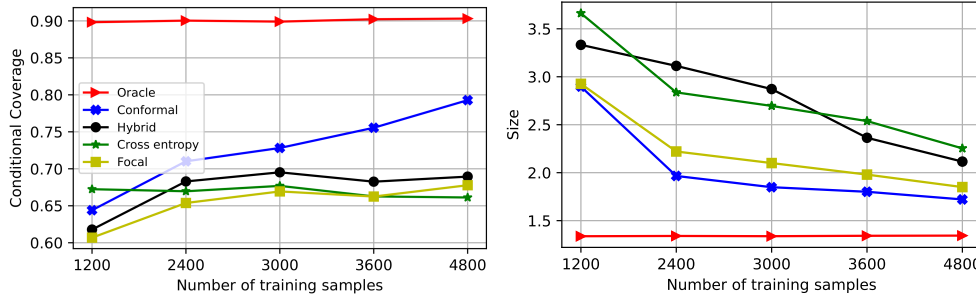


Figure 1: Performance of conformal prediction sets with 90% marginal coverage based on the ideal oracle model and a deep neural network trained with four alternative algorithms. Left: conditional coverage for intrinsically hard samples. Right: average size of prediction sets. The results are averaged over 50 independent experiments and the standard errors are below 0.1 (not shown explicitly).

Figure 1 does not visualize marginal coverage because that is guaranteed to be above 90%. The results show our algorithm yields the prediction sets with highest conditional coverage and smallest size, especially when the number of training samples is large. By contrast, the conditional coverage obtained with the cross entropy does not visibly improve as the training data set grows, suggesting systematic over-confidence with hard-to-classify samples. The focal loss improves upon the cross entropy by reducing the average size of the prediction sets, but it does not lead to higher conditional coverage. Finally, the hybrid algorithm increases conditional coverage slightly compared to the cross entropy, but it does not lead to smaller prediction sets. This is likely because the hybrid loss does not introduce very different incentives compared to the cross entropy, as the latter already attempts to maximize the estimated probability of the observed labels, thus effectively seeking small conformal prediction sets without necessarily high conditional coverage. Note that the focal loss is applied here with hyper-parameter  $\gamma = 1$ , as we have found larger values to yield lower accuracy; see Figure A5.

In this section, our method is applied with the hyper-parameter  $\lambda = 0.2$  in (5); additional results obtained with different values of  $\lambda$  are in Figures A6–A7, Appendix A3.2.

The improved performance of our method can be understood by looking at the distribution of the corresponding conformity scores for test data, as shown in Figure A9 for the model trained on 2400 samples. Our method leads to scores that are more uniformly distributed than those obtained with the cross entropy, which is indicative of more reliable uncertainty quantification. In fact, our estimated conditional probabilities  $\hat{\pi}$  are more similar to the true oracle  $\pi$  compared to those obtained by minimizing the cross entropy; see Figure A10. All figures here refer to fully trained models, without early stopping; analogous results with early stopping are presented later. It is worth emphasizing that post-training conformal calibration is always necessary to guarantee marginal coverage, regardless of how the model is trained. At the same time, it is interesting to observe that models trained with our method tend to estimate more reliable probabilities compared to the benchmarks. Therefore, it should not be surprising that our models lead to larger prediction sets with relatively high marginal coverage if we skip the post-training conformal calibration step; see Figure A8.

Figure A11 compares the performance of the prediction sets obtained with each method when covariate shift occurs in the test data. In particular, here we imagine that at test time the uncertainty-controlling feature  $X_1$  is sampled uniformly from  $[0, a]$  with  $a \leq 1$ , so that lower values of  $a$  correspond to higher proportions of intrinsically hard-to-classify samples. Of course, in this case marginal coverage is no longer guaranteed for the same reason why conditional coverage in Figure 1 is not always controlled. As expected, all models produce smaller set sizes with higher marginal coverage for  $a$  closer to 1, consistently with Figure 1, but our method outperforms the benchmarks.

Several additional results are in Appendix A3.2. Figure A12 reports on experiments in which the number  $K$  of labels is varied, ranging from 4 to 12. These results show our methods leads to prediction sets with consistently smaller size and typically higher conditional coverage compared to all benchmarks. Figure A13 reports on experiments in which the proportion of hard-to-classify samples is varied, ranging from 0.1 to 0.5. All models lead to higher conditional coverage for larger  $\delta$ , as implied by the fixed marginal coverage, but our method consistently achieves it with smaller prediction sets. Figures A14–A17 report on experiments with models trained using early stopping based on maximum prediction accuracy on the validation data. Again, our method achieves higher conditional coverage and smaller prediction sets relative to the benchmarks. Figures A18–A21 report analogous results obtained with early stopping based on minimum validation loss. Figures A22–A23 (resp. A24–A25) show the distribution of conformity scores and the estimated class probabilities, as in Figures A9–A10, from models trained with early stopping based on validation predictive accuracy (resp. loss). Finally, Figures A26–A27 (resp. A28–A29) show the distribution of conformity scores and the estimated class probabilities from the focal loss (res. hybrid) models.

## 4.2 Experiments with CIFAR-10 data

Convolutional neural networks guided by the conformal loss are trained on the publicly available CIFAR-10 image classification data set [81] (10 classes), and the models thus obtained are compared to those targeting the three benchmark losses considered before. As these data are not too hard to classify, we make the problem more interesting by randomly applying RandomErasing [82] to some images—a form of corruption that makes images very hard to recognize. The number of training samples is varied from 3000 to 45000. See Appendix A3.3 for details. To measure the performance of conformal prediction sets based on each model, we set aside 5000 calibration and test observations prior to training. All models are calibrated after training, as in the previous section, in order to guarantee valid marginal coverage. The proportions of corrupt images in the calibration and test sets are 0.2, while that in the training set is varied. All models are calibrated as in [19], seeking 90% marginal coverage. Their performance is measured on the test data in terms of the size of the output prediction sets and their coverage conditional on the indicator of corruption. Further, the test accuracy of each model is evaluated based on the misclassification rate of its best-guess label. Figure 2 showcases two example test images, respectively intact and corrupted by RandomErasing, along with their corresponding conditional class probabilities calculated by different models fully trained on 45000 data points. This shows the model trained with our conformal loss is not as overconfident when dealing with the corrupted images as that minimizing the cross entropy.

Figure A30 summarizes the performance of the prediction sets obtained with each fully trained model, as a function of the number of training samples. Median performance measures are reported over 10

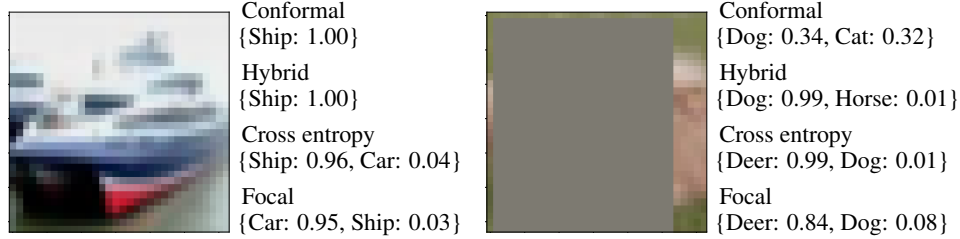


Figure 2: Two example test images from the CIFAR-10 data set, with their top two estimated class probabilities computed by the output softmax layer of convolutional neural networks trained to minimize different loss functions. Left: intact image of a ship. Right: corrupted image of a dog.

experiments with random data subsets. The conformal loss leads to higher coverage for intrinsically hard images, and smaller prediction sets for the easy ones. As shown in Figure A31, this improvement is associated with higher test accuracy for the models targeting our loss, consistently with their increased robustness to overfitting. As overfitting can also be mitigated by early stopping, we report in Figure A32 the corresponding results obtained with early stopping based on maximum accuracy on a validation data set of size 2000 (or 5000, training with 45000 samples). In this case, all models achieve similar test accuracy, but those trained with our method lead to conformal prediction sets with (slightly) higher conditional coverage and smaller size, especially if trained on many samples and compared to the focal loss. These conclusions are summarized in Table 1 in the case of 45000 training samples, which includes also the results corresponding to models trained with early stopping based on validation accuracy. See Table A3 for results with early stopping based on validation loss. Overall, the models targeting the conformal loss perform best when trained fully or with early stopping based on accuracy, and they tend to achieve higher coverage for the hard images while enabling smaller prediction sets with valid coverage for the easy cases. A similar summary for the models trained with 3000 samples is in Table A4; there, the advantage of the conformal loss compared to the hybrid method is not as marked as in the large-sample experiments. Note that the models in Table 1 have accuracy below 83% due to the corrupted images in the training data; by comparison, 89% accuracy could be achieved by applying the cross-entropy method on the clean data set [83].

In Appendix A3.4, Figures A33 and A34 report on results similar to those in Figures A30 and A32, respectively, but using prediction sets directly constructed based on the probability estimates computed by each model, without conformal calibration. Consistently with the experiments described in the previous section, these results show our models lead to prediction sets with relatively high marginal coverage, especially if the sample size is large. Of course, post-training conformal calibration remains necessary to guarantee the nominal coverage level in finite samples. Figures A35 and A36 visualize some concrete examples of prediction sets obtained with and without post-training conformal calibration, respectively for intact and corrupt images. These results confirm the prediction sets obtained with our method tend to be less overconfident compared to the benchmarks, whether or not post-training conformal calibration is applied to guarantee marginal coverage.

	Coverage intact/corrupted		Size intact/corrupted		Accuracy intact/corrupted	
	Full	ES (acc)	Full	ES (acc)	Full	ES (acc)
Conformal	0.90/0.90	0.90/0.87	1.41/5.95	1.41/6.09	0.81/0.35	0.81/0.35
Hybrid	0.92/0.81	0.91/0.86	5.54/5.75	1.38/5.30	0.65/0.40	0.83/0.37
Cross Entropy	0.92/0.84	0.92/0.81	3.30/4.43	1.50/5.05	0.68/0.43	0.82/0.36
Focal	0.91/0.83	0.93/0.77	2.57/3.99	1.91/4.25	0.68/0.42	0.77/0.34

Table 1: Conditional coverage and size of conformal prediction sets with 90% marginal coverage on CIFAR-10 data, based on models trained on 45000 data points. The models are trained either fully for many epochs, or with early stopping (ES) based on classification accuracy (acc). The last two columns report the best-guess classification accuracy of the underlying models applied to test data.

Figure A37 reports performance measures as in Figure A30, after fixing the number of training samples to 45000 and varying the corruption proportion. The model trained with the conformal

loss leads to smaller prediction sets with higher conditional coverage compared to the benchmarks, and its test accuracy does not decrease as the proportion of corrupted training images increases. Figure A38 demonstrates early stopping mitigates overfitting and allows the benchmarks to maintain relatively high accuracy as the training corruption proportion increases. However, the conformal loss outperforms even if all models are trained with early stopping based on validation accuracy. Figure 3 reports on experiments similar to those in Table 1 but performed under covariate shift. Here, the proportions of corrupt images in the training and calibration data sets are still fixed to 0.2, while the proportion of corrupt images in the test set is varied from 0.2 (no covariate shift) to 1.0 (extreme covariate shift). In these experiments, no model is theoretically guaranteed to achieve valid marginal coverage due to the covariate shift, but the model trained with our method remains approximately valid because it has practically high conditional coverage. In conclusion, these results confirm the model trained with our method can provide reliable uncertainty estimates for both intact and the corrupt images, while the benchmark models tend to be overconfident in the hard-to-classify cases.

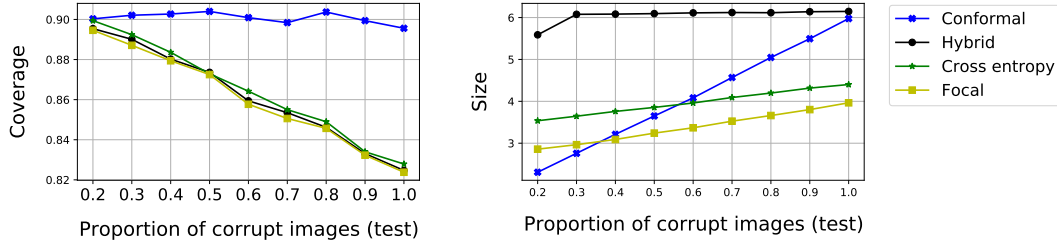


Figure 3: Marginal coverage and average size of conformal prediction sets obtained with models trained by different methods, on the CIFAR-10 data under covariate shift. The results are shown as a function of the proportion of corrupt images in the test set. Other details are as in Table 1.

The distributions of conformity scores obtained with different methods on test data are compared in Figures A39–A42. These results confirm the scores obtained with the conformal loss tend to be more uniform compared to the benchmarks, especially if the training sample size is large. If few training samples are available, the focal loss yields scores that are slightly closer to being uniform, but at the cost of lower accuracy and conditional coverage (Table A4). In Figures A43–A46, the performances of all models are compared separately for each of the 10 possible test labels. These results suggest corrupt images with true labels 4, 5, or 6 are most difficult to classify, and their prediction sets have the lowest coverage. However, this issue is mitigated by models fully trained to minimize the proposed conformal loss. Further, the results confirm that models trained with our loss yield more informative prediction sets for the easier unperturbed images, while achieving the desired coverage rate.

### 4.3 Experiments with credit card data

In this section, we analyze a publicly available credit card default data set [84] containing 30000 observations of 23 features and a binary label. Approximately 22% of the labels are equal to 1. The data are randomly divided into 16800 training samples, 4500 calibration samples, and 4500 test samples, while the remaining 4200 samples are utilized to determine early stopping rules. All experiments are repeated 20 times with independent data subsets. The conformal and hybrid losses are implemented using 70% of the training samples for evaluating the cross entropy component. The model architecture is as in Section 4.1; see Appendix A3.5 for further implementation details.

The performances of conformal prediction sets for models trained with different losses are measured in terms of their respective sizes and coverage conditional on the true label being equal to 1. As the samples with label 1 are a minority, constructing prediction sets with valid coverage for their group is an interesting problem that may be relevant in the context of algorithmic fairness [20]. Note that it is possible to *calibrate* conformal prediction sets in such a way as to achieve perfect label-conditional coverage [17, 19], at the cost of higher data usage, but here we focus on *training* uncertainty-aware models as to approximately achieve this goal without explicit label-conditional calibration. Therefore, we apply a slightly modified version of Algorithm 1 in which the empirical distribution of the hold-out conformity scores is evaluated separately on the samples from each class, and then the sum of these two instances of (7) is utilized as  $\ell_u$ . The same strategy is also incorporated into the hybrid method.

Table 2 compares the average performances of each model and shows our method achieves the highest conditional coverage. Here, early stopping is applied based on minimum validation loss, as the alternative accuracy criterion achieved lower conditional coverage for all models. Our conformal models have relatively high classification errors on these data, but this can be explained by the high class imbalance. Thus, the error rate in Table 2 may be less informative as a performance metric than the corresponding F-score reported in Figure A47, which is higher (better) for the models trained with our method. Finally, Figure A48 and Table A5 in Appendix A3.6 demonstrate our model leads to conformity scores that are closer to being uniformly distributed on test data, as expected.

	Coverage				Size all labels/0/1		Classification error	
	Marginal		Conditional		Full	ES	Full	ES
	Full	ES	Full	ES				
Conformal	0.83	0.83	0.60	0.52	1.34/1.31/1.45	1.29/1.27/1.39	33.05	28.52
Hybrid	0.83	0.83	0.51	0.53	1.27/1.24/1.37	1.28/1.25/1.38	27.00	27.52
Cross Entropy	0.82	0.84	0.51	0.42	1.25/1.23/1.33	1.24/1.21/1.35	26.16	24.36
Focal	0.81	0.82	0.48	0.50	1.22/1.20/1.28	1.25/1.23/1.32	26.56	26.30

Table 2: Performance of conformal prediction sets with 80% marginal coverage on credit card default data, based on convolutional neural networks targeting different losses. Other details are as in Table 1.

## 5 Discussion

The conformal loss function presented in this paper mitigates overconfidence in deep neural networks and can lead to smaller prediction sets with higher conditional coverage compared to standard benchmarks. This contribution is practically relevant for many applications in which overfitting may occur, but it is especially useful when dealing with noisy data that do not allow very accurate out-of-sample predictions. One limitation of the proposed method is that it is more computationally expensive than its benchmarks. For example, training a conformal loss model on 45000 images in the CIFAR-10 data set took us approximately 20 hours on an Nvidia P100 GPU, while training models with the same architecture to minimize the cross entropy or focal loss only took about 11 hours. Another limitation of the conformal loss is that a relatively large number of training samples appears to be required for significant performance improvements. Nonetheless, the ability of an ML model to more openly admit ignorance when asked to provide an unknown answer is a valuable achievement for which it may sometimes be worth investing additional training resources.

Future research may explore extensions of our method for uncertainty-aware learning to problems beyond multi-class classification or to ML models other than deep neural networks, as well as further applications to real-world data sets. Focusing more closely on image classification, it would be interesting to combine the method proposed in this paper with data augmentation techniques that can further increase predictive accuracy [83], especially if the available training set is limited [85]. Further, it could be useful to combine our method with different random image corruption techniques as well as data augmentation in order to improve robustness to covariate shift and adversarial cases. Such extensions are not straightforward because data augmentation may violate the sample exchangeability assumptions, but recent theoretical advances in conformal inference may open the door to a principled solution [86, 87]. We plan to explore these directions in future work.

## Acknowledgements

M. S. and Y. Z. are supported by NSF grant DMS 2210637. M. S. is also supported by an Amazon Research Award. B. E. and Y. R. were supported by the Israel Science Foundation (grant No. 729/21). Y. R. thanks the Career Advancement Fellowship, Technion, for providing research support. The authors also thank four anonymous reviewers for helpful comments and an insightful discussion.

## References

- [1] Jonathan Schmidt, Mário RG Marques, Silvana Botti, and Miguel AL Marques. Recent advances and applications of machine learning in solid-state materials science. *npj Comput. Mater.*, 5(1):

- 1–36, 2019.
- [2] Alexandre Tkatchenko. Machine learning for chemical discovery. *Nat. Commun.*, 11(1):1–4, 2020.
  - [3] Gisbert Schneider. Mind and machine in drug design. *Nat. Mach. Intell.*, 1(3):128–130, 2019.
  - [4] Sorin Grigorescu, Bogdan Trasnea, Tiberiu Cocias, and Gigel Macesanu. A survey of deep learning techniques for autonomous driving. *Journal of Field Robotics*, 37(3):362–386, 2020.
  - [5] Daniel S Hoadley and Nathan J Lucas. Artificial intelligence and national security, 2018.
  - [6] Cynthia Rudin. Stop explaining black box machine learning models for high stakes decisions and use interpretable models instead. *Nat. Mach. Intell.*, 1(5):206–215, 2019.
  - [7] Chuan Guo, Geoff Pleiss, Yu Sun, and Kilian Q Weinberger. On calibration of modern neural networks. In *Proceedings of the 34th International Conference on Machine Learning-Volume 70*, pages 1321–1330. JMLR. org, 2017.
  - [8] Sunil Thulasidasan, Gopinath Chennupati, Jeff A Bilmes, Tanmoy Bhattacharya, and Sarah Michalak. On mixup training: Improved calibration and predictive uncertainty for deep neural networks. In *Adv. Neural. Inf. Process. Syst.*, pages 13888–13899, 2019.
  - [9] Yaniv Ovadia, Emily Fertig, Jie Ren, Zachary Nado, David Sculley, Sebastian Nowozin, Joshua Dillon, Balaji Lakshminarayanan, and Jasper Snoek. Can you trust your model’s uncertainty? evaluating predictive uncertainty under dataset shift. In *Adv. Neural. Inf. Process. Syst.*, pages 13991–14002, 2019.
  - [10] Eyke Hüllermeier and Willem Waegeman. Aleatoric and epistemic uncertainty in machine learning: An introduction to concepts and methods. *Machine Learning*, 110(3):457–506, 2021.
  - [11] Chansik An, Hyunsun Lim, Dong-Wook Kim, Jung Hyun Chang, Yoon Jung Choi, and Seong Woo Kim. Machine learning prediction for mortality of patients diagnosed with covid-19: a nationwide korean cohort study. *Scientific Reports*, 10(1):18716, 2020. ISSN 2045-2322.
  - [12] Yue Gao, Guang-Yao Cai, Wei Fang, Hua-Yi Li, Si-Yuan Wang, Lingxi Chen, Yang Yu, Dan Liu, Sen Xu, Peng-Fei Cui, Shao-Qing Zeng, Xin-Xia Feng, Rui-Di Yu, Ya Wang, Yuan Yuan, Xiao-Fei Jiao, Jian-Hua Chi, Jia-Hao Liu, Ru-Yuan Li, Xu Zheng, Chun-Yan Song, Ning Jin, Wen-Jian Gong, Xing-Yu Liu, Lei Huang, Xun Tian, Lin Li, Hui Xing, Ding Ma, Chun-Rui Li, Fei Ye, and Qing-Lei Gao. Machine learning based early warning system enables accurate mortality risk prediction for covid-19. *Nat. Commun.*, 11(1):5033, 2020. ISSN 2041-1723.
  - [13] Michela Carlotta Massi, Francesca Gasperoni, Francesca Ieva, Anna Maria Paganoni, Paolo Zunino, Andrea Manzoni, Nicola Rares Franco, Liv Veldeman, Piet Ost, Valérie Fonteyne, et al. A deep learning approach validates genetic risk factors for late toxicity after prostate cancer radiotherapy in a requisite multi-national cohort. *Frontiers in oncology*, 10, 2020.
  - [14] Adrien Badré, Li Zhang, Wellington Muchero, Justin C Reynolds, and Chongle Pan. Deep neural network improves the estimation of polygenic risk scores for breast cancer. *Journal of Human Genetics*, 66(4):359–369, 2021.
  - [15] Arno van Hilten, Steven A Kushner, Manfred Kayser, M Arfan Ikram, Hieab HH Adams, Caroline CW Klaver, Wiro J Niessen, and Gennady V Roshchupkin. Gennet framework: interpretable deep learning for predicting phenotypes from genetic data. *Communications biology*, 4(1):1–9, 2021.
  - [16] Ting Sun and Miklos A Vasarhelyi. Predicting credit card delinquencies: An application of deep neural networks. In *Handbook of Financial Econometrics, Mathematics, Statistics, and Machine Learning*, pages 4349–4381. World Scientific, 2021.
  - [17] Vladimir Vovk, Alex Gammerman, and Glenn Shafer. *Algorithmic learning in a random world*. Springer, 2005.
  - [18] Maxime Cauchois, Suyash Gupta, and John Duchi. Knowing what you know: valid confidence sets in multiclass and multilabel prediction. *arXiv:2004.10181*, 2020.

- [19] Yaniv Romano, Matteo Sesia, and Emmanuel J. Candès. Classification with valid and adaptive coverage. In *Adv. Neural. Inf. Process. Syst.*, 2020.
- [20] Yaniv Romano, Rina Foygel Barber, Chiara Sabatti, and Emmanuel Candès. With malice toward none: Assessing uncertainty via equalized coverage. *Harvard Data Science Review*, 2020.
- [21] Marten Wegkamp. Lasso type classifiers with a reject option. *Electron. J. Statist.*, 1:155–168, 2007.
- [22] Yves Grandvalet, Alain Rakotomamonjy, Joseph Keshet, and Stéphane Canu. Support vector machines with a reject option. In *Adv. Neural. Inf. Process. Syst.*, pages 537–544, 2009.
- [23] Corinna Cortes, Giulia DeSalvo, and Mehryar Mohri. Boosting with abstention. In *Adv. Neural. Inf. Process. Syst.*, pages 1660–1668, 2016.
- [24] Cláudio Rebelo de Sá, Carlos Soares, Arno Knobbe, and Paulo Cortez. Label ranking forests. *Expert systems*, 34(1):e12166, 2017.
- [25] Leying Guan and Rob Tibshirani. Prediction and outlier detection in classification problems. *preprint arXiv:1905.04396*, 2019.
- [26] Peter L Bartlett and Marten H Wegkamp. Classification with a reject option using a hinge loss. *J. Mach. Learn. Res.*, 9:1823–1840, 2008.
- [27] Juan José Del Coz, Jorge Díez, and Antonio Bahamonde. Learning nondeterministic classifiers. *J. Mach. Learn. Res.*, 10(10), 2009.
- [28] Yair Wiener and Ran El-Yaniv. Agnostic selective classification. In *Adv. Neural. Inf. Process. Syst.*, pages 1665–1673, 2011.
- [29] Heinrich Jiang, Been Kim, Melody Guan, and Maya Gupta. To trust or not to trust a classifier. In *Adv. Neural. Inf. Process. Syst.*, pages 5541–5552, 2018.
- [30] Yotam Hechtlinger, Barnabás Póczos, and Larry Wasserman. Cautious deep learning. *arXiv:1805.09460*, 2018.
- [31] Ziyin Liu, Zhikang Wang, Paul Pu Liang, Russ R Salakhutdinov, Louis-Philippe Morency, and Masahito Ueda. Deep gamblers: Learning to abstain with portfolio theory. In *Adv. Neural. Inf. Process. Syst.*, pages 10623–10633, 2019.
- [32] Ron Slossberg, Oron Anschel, Amir Markovitz, Ron Litman, Aviad Aberdam, Shahar Tsiper, Shai Mazor, Jon Wu, and R Manmatha. On calibration of scene-text recognition models. *arXiv preprint arXiv:2012.12643*, 2020.
- [33] Lijing Wang, Dipanjan Ghosh, Maria Gonzalez Diaz, Ahmed Farahat, Mahbubul Alam, Chetan Gupta, Jiangzhuo Chen, and Madhav Marathe. Wisdom of the ensemble: Improving consistency of deep learning models. *Advances in Neural Information Processing Systems*, 33:19750–19761, 2020.
- [34] Sijie Yan, Yuanjun Xiong, Kaustav Kundu, Shuo Yang, Siqi Deng, Meng Wang, Wei Xia, and Stefano Soatto. Positive-congruent training: Towards regression-free model updates. In *Proceedings of the IEEE/CVF Conference on Computer Vision and Pattern Recognition*, pages 14299–14308, 2021.
- [35] John Platt. Probabilistic outputs for support vector machines and comparisons to regularized likelihood methods. *Advances in large margin classifiers*, 10(3):61–74, 1999.
- [36] Bianca Zadrozny and Charles Elkan. Obtaining calibrated probability estimates from decision trees and naive bayesian classifiers. In *Icml*, volume 1, pages 609–616. Citeseer, 2001.
- [37] Bianca Zadrozny and Charles Elkan. Transforming classifier scores into accurate multiclass probability estimates. In *Proceedings of the eighth ACM SIGKDD international conference on Knowledge discovery and data mining*, pages 694–699, 2002.

- [38] Charles Blundell, Julien Cornebise, Koray Kavukcuoglu, and Daan Wierstra. Weight uncertainty in neural network. In Francis Bach and David Blei, editors, *Proceedings of the 32nd International Conference on Machine Learning*, volume 37 of *Proceedings of Machine Learning Research*, pages 1613–1622, Lille, France, 2015. PMLR.
- [39] Juozas Vaicenavicius, David Widmann, Carl Andersson, Fredrik Lindsten, Jacob Roll, and Thomas Schön. Evaluating model calibration in classification. In Kamalika Chaudhuri and Masashi Sugiyama, editors, *Proceedings of Machine Learning Research*, volume 89 of *Proceedings of Machine Learning Research*, pages 3459–3467. PMLR, 2019.
- [40] Lukas Neumann, Andrew Zisserman, and Andrea Vedaldi. Relaxed softmax: Efficient confidence auto-calibration for safe pedestrian detection, 2018.
- [41] Lutz Prechelt. Early stopping-but when? In *Neural Networks: Tricks of the trade*, pages 55–69. Springer, 1998.
- [42] Antonio Bella, Cèsar Ferri, José Hernández-Orallo, and María José Ramírez-Quintana. Calibration of machine learning models. In *Handbook of Research on Machine Learning Applications and Trends: Algorithms, Methods, and Techniques*, pages 128–146. IGI Global, 2010.
- [43] Yarin Gal. Uncertainty in deep learning. *University of Cambridge*, 1(3), 2016.
- [44] Balaji Lakshminarayanan, Alexander Pritzel, and Charles Blundell. Simple and scalable predictive uncertainty estimation using deep ensembles. In *Adv. Neural. Inf. Process. Syst.*, pages 6402–6413, 2017.
- [45] Ananya Kumar, Percy S Liang, and Tengyu Ma. Verified uncertainty calibration. In *Adv. Neural. Inf. Process. Syst.*, pages 3787–3798, 2019.
- [46] Natasa Tagasovska and David Lopez-Paz. Single-model uncertainties for deep learning. In *Adv. Neural. Inf. Process. Syst.*, pages 6417–6428, 2019.
- [47] Yonatan Geifman and Ran El-Yaniv. Selectivenet: A deep neural network with an integrated reject option. In *International Conference on Machine Learning*, pages 2151–2159, 2019.
- [48] Wesley J Maddox, Pavel Izmailov, Timur Garipov, Dmitry P Vetrov, and Andrew Gordon Wilson. A simple baseline for bayesian uncertainty in deep learning. In *Adv. Neural. Inf. Process. Syst.*, pages 13153–13164, 2019.
- [49] José Mena, Oriol Pujol, and Jordi Vitrià. Uncertainty-based rejection wrappers for black-box classifiers. *IEEE Access*, 2020.
- [50] Yukun Ding, Jinglan Liu, Xiaowei Xu, Meiping Huang, Jian Zhuang, Jinjun Xiong, and Yiyu Shi. Uncertainty-aware training of neural networks for selective medical image segmentation. In *Medical Imaging with Deep Learning*, 2020.
- [51] Biraja Ghoshal and Allan Tucker. Estimating uncertainty and interpretability in deep learning for coronavirus (covid-19) detection. *arXiv:2003.10769*, 2020.
- [52] Eli Simhayev, Gilad Katz, and Lior Rokach. PIVEN: A deep neural network for prediction intervals with specific value prediction. *arXiv:2006.05139*, 2020.
- [53] Jing Lei, James Robins, and Larry Wasserman. Distribution-free prediction sets. *J. Am. Stat. Assoc.*, 108(501):278–287, 2013.
- [54] Jing Lei and Larry Wasserman. Distribution-free prediction bands for non-parametric regression. *J. Royal Stat. Soc. B*, 76(1):71–96, 2014.
- [55] Jing Lei, Max G’Sell, Alessandro Rinaldo, Ryan J Tibshirani, and Larry Wasserman. Distribution-free predictive inference for regression. *J. Am. Stat. Assoc.*, 113(523):1094–1111, 2018.
- [56] Rina Foygel Barber, Emmanuel J Candès, Aaditya Ramdas, and Ryan J Tibshirani. Predictive inference with the jackknife+. *The Annals of Statistics*, 49(1):486–507, 2021.

- [57] Ryan J Tibshirani, Rina Foygel Barber, Emmanuel Candès, and Aaditya Ramdas. Conformal prediction under covariate shift. *Advances in neural information processing systems*, 32, 2019.
- [58] Yaniv Romano, Evan Patterson, and Emmanuel J Candès. Conformalized quantile regression. In *Adv. Neural. Inf. Process. Syst.*, pages 3538–3548, 2019.
- [59] Anastasios Angelopoulos, Stephen Bates, Jitendra Malik, and Michael I Jordan. Uncertainty sets for image classifiers using conformal prediction. *arXiv preprint arXiv:2009.14193*, 2020.
- [60] Stephen Bates, Anastasios Angelopoulos, Lihua Lei, Jitendra Malik, and Michael Jordan. Distribution-free, risk-controlling prediction sets. *Journal of the ACM (JACM)*, 68(6):1–34, 2021.
- [61] Nicolo Colombo and Vladimir Vovk. Training conformal predictors. In *Conformal and Probabilistic Prediction and Applications*, pages 55–64. PMLR, 2020.
- [62] Anthony Bellotti. Optimized conformal classification using gradient descent approximation. *arXiv preprint arXiv:2105.11255*, 2021.
- [63] David Stutz, Ali Taylan Cemgil, Arnaud Doucet, et al. Learning optimal conformal classifiers. *arXiv preprint arXiv:2110.09192*, 2021.
- [64] Haoxian Chen, Ziyi Huang, Henry Lam, Huajie Qian, and Haofeng Zhang. Learning prediction intervals for regression: Generalization and calibration. In *International Conference on Artificial Intelligence and Statistics*, pages 820–828. PMLR, 2021.
- [65] Yachong Yang and Arun Kumar Kuchibhotla. Finite-sample efficient conformal prediction. *arXiv preprint arXiv:2104.13871*, 2021.
- [66] Yu Bai, Song Mei, Huan Wang, Yingbo Zhou, and Caiming Xiong. Efficient and differentiable conformal prediction with general function classes. *arXiv preprint arXiv:2202.11091*, 2022.
- [67] Matteo Sesia and Yaniv Romano. Conformal prediction using conditional histograms. In *Adv. Neural. Inf. Process. Syst.*, volume 34, 2021.
- [68] Anastasios N Angelopoulos, Amit P Kohli, Stephen Bates, Michael I Jordan, Jitendra Malik, Thayer Alshaabi, Srigoikul Upadhyayula, and Yaniv Romano. Image-to-image regression with distribution-free uncertainty quantification and applications in imaging. *arXiv preprint arXiv:2202.05265*, 2022.
- [69] Matteo Sesia and Stefano Favaro. Conformalized frequency estimation from sketched data. *arXiv preprint arXiv:2204.04270*, 2022.
- [70] Stephen Bates, Emmanuel Candès, Lihua Lei, Yaniv Romano, and Matteo Sesia. Testing for outliers with conformal p-values. *arXiv preprint arXiv:2104.08279*, 2021.
- [71] Vladimir Vovk. Conditional validity of inductive conformal predictors. In *Asian conference on machine learning*, pages 475–490, 2012.
- [72] Rina Foygel Barber, Emmanuel J Candès, Aaditya Ramdas, and Ryan J Tibshirani. The limits of distribution-free conditional predictive inference. *Information and Inference: A Journal of the IMA*, 10(2):455–482, 2021.
- [73] Marco Cuturi, Olivier Teboul, and Jean-Philippe Vert. Differentiable ranking and sorting using optimal transport. In *Adv. Neural. Inf. Process. Syst.*, pages 6861–6871, 2019.
- [74] Mathieu Blondel, Olivier Teboul, Quentin Berthet, and Josip Djolonga. Fast differentiable sorting and ranking, 2020.
- [75] Harald Cramér. On the composition of elementary errors: First paper: Mathematical deductions. *Scandinavian Actuarial Journal*, 1928(1):13–74, 1928.
- [76] Richard Von Mises. Statistik und wahrheit. *Julius Springer*, 20, 1928.

- [77] Nikolai V Smirnov. Estimate of deviation between empirical distribution functions in two independent samples. *Bulletin Moscow University*, 2(2):3–16, 1939.
- [78] Frank J. Massey Jr. The kolmogorov-smirnov test for goodness of fit. *J. Am. Stat. Assoc.*, 46(253):68–78, 1951.
- [79] Adam Paszke, Sam Gross, Francisco Massa, Adam Lerer, James Bradbury, Gregory Chanan, Trevor Killeen, Zeming Lin, Natalia Gimelshein, Luca Antiga, et al. Pytorch: An imperative style, high-performance deep learning library. *Advances in neural information processing systems*, 32, 2019.
- [80] Jishnu Mukhoti, Viveka Kulharia, Amartya Sanyal, Stuart Golodetz, Philip Torr, and Puneet Dokania. Calibrating deep neural networks using focal loss. *Advances in Neural Information Processing Systems*, 33:15288–15299, 2020.
- [81] Alex Krizhevsky, Vinod Nair, and Geoffrey Hinton. CIFAR-10 data set, 2009. URL <http://www.cs.toronto.edu/~kriz/cifar.html>.
- [82] Zhun Zhong, Liang Zheng, Guoliang Kang, Shaozi Li, and Yi Yang. Random erasing data augmentation. In *Proceedings of the AAAI conference on artificial intelligence*, volume 34, pages 13001–13008, 2020.
- [83] Connor Shorten and Taghi M Khoshgoftaar. A survey on image data augmentation for deep learning. *Journal of big data*, 6(1):1–48, 2019.
- [84] I-Cheng Yeh and Che-hui Lien. The comparisons of data mining techniques for the predictive accuracy of probability of default of credit card clients. *Expert systems with applications*, 36(2): 2473–2480, 2009.
- [85] Tero Karras, Miika Aittala, Janne Hellsten, Samuli Laine, Jaakko Lehtinen, and Timo Aila. Training generative adversarial networks with limited data. *Advances in Neural Information Processing Systems*, 33:12104–12114, 2020.
- [86] Rina Foygel Barber, Emmanuel J Candes, Aaditya Ramdas, and Ryan J Tibshirani. Conformal prediction beyond exchangeability. *arXiv preprint arXiv:2202.13415*, 2022.
- [87] Robin Dunn, Larry Wasserman, and Aaditya Ramdas. Distribution-free prediction sets for two-layer hierarchical models. *Journal of the American Statistical Association*, pages 1–12, 2022.
- [88] Saeed Ghadimi and Guanghui Lan. Stochastic first-and zeroth-order methods for nonconvex stochastic programming. *SIAM Journal on Optimization*, 23(4):2341–2368, 2013.
- [89] Maziar Sanjabi, Jimmy Ba, Meisam Razaviyayn, and Jason D Lee. Solving approximate wasserstein gans to stationarity. *arXiv preprint arXiv:1802.08249*, 2018.
- [90] Yaniv Romano, Matteo Sesia, and Emmanuel Candès. Deep knockoffs. *J. Am. Stat. Assoc.*, 0(ja):1–27, 2019.
- [91] Aryeh Dvoretzky, Jack Kiefer, and Jacob Wolfowitz. Asymptotic minimax character of the sample distribution function and of the classical multinomial estimator. *The Annals of Mathematical Statistics*, pages 642–669, 1956.
- [92] Diederik P Kingma and Jimmy Ba. Adam: A method for stochastic optimization. *arXiv preprint arXiv:1412.6980*, 2014.
- [93] Kaiming He, Xiangyu Zhang, Shaoqing Ren, and Jian Sun. Deep residual learning for image recognition. In *Proceedings of the IEEE conference on computer vision and pattern recognition*, pages 770–778, 2016.

## A1 Additional methodological details

### A1.1 Conformity scores for multi-class classification

For any  $\tau \in [0, 1]$ , define as in [20] the *generalized conditional quantile* function:

$$L(x; \pi, \tau) = \min\{k \in \{1, \dots, K\} : \pi_{(1)}(x) + \pi_{(2)}(x) + \dots + \pi_{(k)}(x) \geq \tau\}. \quad (\text{A9})$$

Then, recall from that, for any  $\tau \in [0, 1]$  and  $u \in (0, 1)$ , the function with input  $x$ ,  $u$ ,  $\pi$ , and  $\tau$  that computes the set of most likely labels up to (but possibly excluding) the one identified by the deterministic oracle in Section 2.2 is:

$$\mathcal{S}(x, u; \pi, \tau) = \begin{cases} \text{'y' indices of the } L(x; \pi, \tau) - 1 \text{ largest } \pi_y(x), & \text{if } u \leq V(x; \pi, \tau), \\ \text{'y' indices of the } L(x; \pi, \tau) \text{ largest } \pi_y(x), & \text{otherwise,} \end{cases} \quad (\text{A10})$$

$$V(x; \pi, \tau) = \frac{1}{\pi_{(L(x; \pi, \tau))}(x)} \left[ \sum_{k=1}^{L(x; \pi, \tau)} \pi_{(k)}(x) - \tau \right],$$

where  $\pi_{(1)}(x) \geq \pi_{(2)}(x) \geq \dots \geq \pi_{(K)}(x)$  are the order statistics of  $\hat{\pi}_1(x), \dots, \hat{\pi}_K(x)$ . Note that it is typically preferable to skip the randomization step in (A10) if  $L(x; \pi, \tau) = 1$ , to avoid returning empty prediction sets.

The conformity scores defined in (4) are not differentiable in the model parameters  $\theta$  because they involve ranking and sorting the estimated class probabilities  $\hat{\pi}$ . In fact,  $Y_i \in \mathcal{S}(X_i, U_i; \hat{\pi}, \tau)$ , where  $\mathcal{S}$  is defined as in (A10), if and only if  $U_i \geq V(X_i; \hat{\pi}, \tau)$ . This means that  $Y_i \in \mathcal{S}(X_i, U_i; \hat{\pi}, \tau)$  if and only if  $\tau \geq \hat{\pi}_{(1)}(X_i) + \hat{\pi}_{(2)}(X_i) + \dots + \hat{\pi}_{(r(Y_i, \hat{\pi}(X_i)))}(X_i) - U_i \cdot \hat{\pi}_{(r(Y_i, \hat{\pi}(X_i)))}(X_i)$ , where  $r(Y_i, \hat{\pi}(X_i))$  denotes the rank of  $\hat{\pi}_{Y_i}(X_i)$  among  $\hat{\pi}_1(X_i), \dots, \hat{\pi}_K(X_i)$ . Therefore, the conformity scores can be written as in (8):

$$W_i = \hat{\pi}_{(1)}(X_i) + \hat{\pi}_{(2)}(X_i) + \dots + \hat{\pi}_{(r(Y_i, \hat{\pi}(X_i)))}(X_i) - U_i \cdot \hat{\pi}_{(r(Y_i, \hat{\pi}(X_i)))}(X_i), \quad (\text{A11})$$

where  $U_i$  is a uniform random variable independent of everything else.

### A1.2 Further details on the conformal learning algorithm

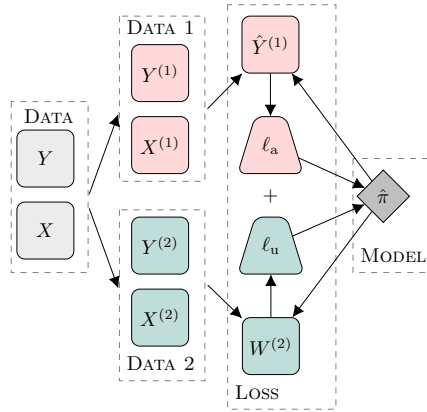


Figure A4: Schematic of the proposed uncertainty-aware deep classification learning algorithm. The training data are split into two subsets. The first subset (in red) is utilized to evaluate a traditional accuracy-based loss function  $\ell_a$ , such as the cross entropy. The second subset (in green) is utilized to evaluate the deviation from uniformity of the distribution of the model's conformity scores  $W$ , which is approximated by a differentiable loss function  $\ell_u$ . The overall additive loss is minimized through gradient descent. The output of the final soft-max layer in the trained model can be interpreted as a more reliable estimate of conditional class probabilities.

Here we explain in detail the implementation of the differentiable loss function  $\tilde{\ell}_u$  in Algorithm 1. The function  $\tilde{\ell}_u$  takes as input the estimated probabilities for the  $i$ -th data point as output by the soft-max

layer of the model, namely  $[\hat{\pi}_1(X_i), \hat{\pi}_2(X_i), \dots, \hat{\pi}_K(X_i)]$ , as well as the corresponding label,  $Y_i$ . The estimated probabilities are soft-sorted, yielding an array  $[\tilde{\pi}_{(1)}(X_i), \tilde{\pi}_{(2)}(X_i), \dots, \tilde{\pi}_{(K)}(X_i)]$  that approximates the order statistics  $[\hat{\pi}_{(1)}(X_i), \hat{\pi}_{(2)}(X_i), \dots, \hat{\pi}_{(K)}(X_i)]$ . Similarly, the estimated probabilities are also soft-ranked, yielding an array  $[\tilde{r}(1, \hat{\pi}(X_i)), \tilde{r}(2, \hat{\pi}(X_i)), \dots, \tilde{r}(K, \hat{\pi}(X_i))]$  that takes continuous values in the interval  $[1, K]$  and approximates the true label ranks  $[\hat{r}(1, \hat{\pi}(X_i)), \hat{r}(2, \hat{\pi}(X_i)), \dots, \hat{r}(K, \hat{\pi}(X_i))]$ .

To evaluate the differentiable conformity scores  $\tilde{W}_i$ , we begin by computing a soft approximation of the estimated conditional CDF of the observed label; this is achieved by taking the cumulative sum of  $[\tilde{\pi}_{(1)}(X_i), \tilde{\pi}_{(2)}(X_i), \dots, \tilde{\pi}_{(K)}(X_i)]$ . Then, we approximate the value of the CDF at the true label  $Y_i$  by soft-indexing the differentiable approximation of the CDF obtained above, obtaining an approximation  $\tilde{\pi}_{(1)}(X_i) + \tilde{\pi}_{(2)}(X_i) + \dots + \tilde{\pi}_{(\tilde{r}(Y_i, \hat{\pi}(X_i)))}(X_i)$  of  $\hat{\pi}_{(1)}(X_i) + \hat{\pi}_{(2)}(X_i) + \dots + \hat{\pi}_{(\hat{r}(Y_i, \hat{\pi}(X_i)))}(X_i)$ . This soft-indexing operation needs to operate with a continuous-valued index and simply consists of a smooth linear interpolation of the target array. Next, we apply soft-sorting to also compute the estimated probability of the observed label,  $\tilde{\pi}_{(\tilde{r}(Y_i, \hat{\pi}(X_i)))}(X_i)$ . Thus, the differentiable approximation of the conformity score in (A11) is given by:

$$\tilde{W}_i = \tilde{\pi}_{(1)}(X_i) + \tilde{\pi}_{(2)}(X_i) + \dots + \tilde{\pi}_{(\tilde{r}(Y_i, \hat{\pi}(X_i)))}(X_i) - U_i \cdot \tilde{\pi}_{(\tilde{r}(Y_i, \hat{\pi}(X_i)))}(X_i), \quad (\text{A12})$$

where  $U_i$  is a uniform random variable independent of everything else.

Finally, we need a differentiable approximation of the Kolmogorov-Smirnov deviation from uniformity of the differentiable conformity scores  $\tilde{W}_i$  obtained above. For this purpose, we compute a smooth version of the empirical CDF of  $\tilde{W}_i$  for all  $i \in \mathcal{I}_2$ ; this is achieved by viewing the CDF as a sum of  $|\mathcal{I}_2|$  indicator functions, each of which is approximated smoothly using two sigmoid functions. Then, we can obtain a differentiable approximation of the Kolmogorov-Smirnov distance from the uniform distribution by simply taking the maximum distance between the above approximate CDF and the uniform CDF. This procedure is summarized in Algorithm A2, which is a more technical version of Algorithm 1. For further implementation details, we refer our open-source software available online at <https://github.com/bat-sheva/conformal-learning>.

---

**Algorithm A2:** Conformalized uncertainty-aware training of deep multi-class classifiers

---

**Input:** Data  $\{X_i, Y_i\}_{i=1}^n$ ; hyper-parameter  $\lambda \in [0, 1]$ , learning rate  $\gamma > 0$ , batch size  $M$ ;

Randomly initialize the model parameters  $\theta^{(0)}$ ;

Randomly split the data into two disjoint subsets,  $\mathcal{I}_1, \mathcal{I}_2$ , such that  $\mathcal{I}_1 \cup \mathcal{I}_2 = [n]$ ;

Set the number of batches to  $B = (n/2)/M$  (assuming for simplicity that  $|\mathcal{I}_1| = |\mathcal{I}_2|$ );

**for**  $t = 1, \dots, T$  **do**

    Randomly divide  $\mathcal{I}_1$  and  $\mathcal{I}_2$  into  $B$  batches;

**for**  $b = 1, \dots, B$  **do**

        Evaluate (softmax) conditional probabilities  $\hat{\pi}(X_i)$  for all  $i$  in batch  $b$  of  $\mathcal{I}_1 \cup \mathcal{I}_2$ ;

        Evaluate the gradient  $\nabla \ell_a(\theta^{(t)})$  of  $\ell_a$  in (6) using the data in batch  $b$  of  $\mathcal{I}_1$ ;

**for**  $i$  in batch  $b$  of  $\mathcal{I}_2$  **do**

            Generate a uniform independent random variable  $U_i$ ;

            Soft-sort the estimated probabilities output by the soft-max layer;

            Sum the soft-sorted probabilities to approximate the CDF of  $Y \mid X_i$ ;

            Approximate the rank of  $Y_i$  based on the estimated probabilities using soft-ranking;

            Approximate the CDF of the labels at the observed  $Y_i$  with soft-indexing;

            Approximate the probability of the observed  $Y_i$  with soft-indexing;

            Evaluate differentiable conformity scores  $\tilde{W}_i$  with (A12).

**end**

        Approximate the CDF of  $\tilde{W}_i$  for all  $i$  in batch  $b$  of  $\mathcal{I}_2$  using a sum of sigmoid functions;

        Compute  $\tilde{\ell}_u$  as the max distance between the above smooth CDF and the uniform CDF;

        Evaluate the gradient  $\nabla \tilde{\ell}_u(\theta^{(t)})$  of  $\tilde{\ell}_u$ ;

        Define the total gradient  $\nabla \tilde{\ell}(\theta^{(t)}) = (1 - \lambda) \cdot \nabla \ell_a(\theta^{(t)}) + \lambda \cdot \nabla \tilde{\ell}_u(\theta^{(t)})$  based on (5);

        Update the model parameters:  $\theta^{(t)} \leftarrow \theta^{(t-1)} - \gamma \nabla \tilde{\ell}(\theta^{(t-1)})$ .

**end**

**end**

**Output:** The model  $\hat{\pi}$  corresponding to the fitted parameters  $\theta^{(T)}$ .

---

### A1.3 Implementation of the hybrid training algorithm

This section explains the implementation of the hybrid benchmark method applied in Section 4. This benchmark is inspired by the recent proposal of [63], although it may not be able to replicate its performance exactly because a software implementation of the latter has not yet been made available. This benchmark is based on a loss function designed to incentivize the trained model to produce the smallest possible conformal prediction sets with the desired coverage (e.g., 90% if  $\alpha = 0.1$ ). The hybrid training procedure is similar to Algorithm 1, in the sense that it relies on analogous soft-sorting, soft-ranking, and soft-indexing algorithms to evaluate a differentiable approximation  $\tilde{W}_i$  of the conformity score  $W_i$  in (8). However, unlike Algorithm 1, this hybrid method does not compare the distribution of  $\tilde{W}_i$  on hold-out data to the ideal uniform distribution. Instead, for all data points  $X_i$  in the second training subset  $\mathcal{I}_2$ , approximate conformity scores  $\tilde{W}_i$  are computed and then soft-sorted. This gives us an approximation of the  $1 - \alpha$  empirical quantile of  $\tilde{W}_i$ , which can be used to compute a differentiable approximation of the size of the corresponding conformal prediction set (more precisely, we find the rank of the label at which the empirical CDF of  $\tilde{W}_i$  first crosses the  $1 - \alpha$  threshold). Then, a differentiable loss function  $\tilde{\ell}_s$  is defined as the average size of these smoothed conformal prediction sets. This plays the role of  $\tilde{\ell}_u$  in Algorithm 1, as outlined in Algorithm A3.

---

**Algorithm A3:** Hybrid conformalized training of deep multi-class classifiers

---

**Input:** Data  $\{X_i, Y_i\}_{i=1}^n$ ; hyper-parameter  $\lambda \in [0, 1]$ , learning rate  $\gamma > 0$ , batch size  $M$ , desired marginal coverage level  $\alpha \in (0, 1)$ ;

Randomly initialize the model parameters  $\theta^{(0)}$ ;

Randomly split the data into two disjoint subsets,  $\mathcal{I}_1, \mathcal{I}_2$ , such that  $\mathcal{I}_1 \cup \mathcal{I}_2 = [n]$ ;

Set the number of batches to  $B = (n/2)/M$  (assuming for simplicity that  $|\mathcal{I}_1| = |\mathcal{I}_2|$ );

**for**  $t = 1, \dots, T$  **do**

    Randomly divide  $\mathcal{I}_1$  and  $\mathcal{I}_2$  into  $B$  batches;

**for**  $b = 1, \dots, B$  **do**

        Evaluate (softmax) conditional probabilities  $\hat{\pi}(X_i)$  for all  $i$  in batch  $b$  of  $\mathcal{I}_1 \cup \mathcal{I}_2$ ;

        Generate a uniform independent random variable  $U_i$  for all  $i$  in batch  $b$  of  $\mathcal{I}_2$ ;

        Evaluate  $\tilde{W}_i$  for all  $i$  in batch  $b$  of  $\mathcal{I}_2$ , using  $U_i$  and a differentiable approximation of (4);

        Compute a differentiable approximation  $\tilde{S}_i$  of the size of the conformal prediction set for  $X_i$  at level  $1 - \alpha$ , for all  $i$  in batch  $b$  of  $\mathcal{I}_2$ ;

        Define  $\tilde{\ell}_s(\theta^{(t)}) = (1/m) \sum_{i \in \mathcal{I}_2} |\tilde{S}_i|$ , where  $|\cdot|$  is the set size;

        Evaluate the gradient  $\nabla \ell_a(\theta^{(t)})$  of  $\ell_a$  in (6) using the data in batch  $b$  of  $\mathcal{I}_1$ ;

        Evaluate the gradient  $\nabla \tilde{\ell}_s(\theta^{(t)})$  of a differentiable approximation  $\tilde{\ell}_s$  of  $\ell_s$  in (7) using the differentiable scores  $\tilde{W}_i$  in batch  $b$  of  $\mathcal{I}_2$ ;

        Define  $\nabla \tilde{\ell}(\theta^{(t)}) = (1 - \lambda) \cdot \nabla \ell_a(\theta^{(t)}) + \lambda \cdot \nabla \tilde{\ell}_s(\theta^{(t)})$  based on (5);

        Update the model parameters:  $\theta^{(t)} \leftarrow \theta^{(t-1)} - \gamma \nabla \tilde{\ell}(\theta^{(t-1)})$ .

**end**

**end**

**Output:** The model  $\hat{\pi}$  corresponding to the fitted parameters  $\theta^{(T)}$ .

---

## A2 Additional theoretical results

### A2.1 Convergence analysis of Algorithm 1

To facilitate the exposition of our analysis, we begin by introducing some helpful notations. Define  $\mathcal{D}_1 = (X_i, Y_i)_{i \in \mathcal{I}_1}$  and  $\mathcal{D}_2 = (X_i, Y_i)_{i \in \mathcal{I}_2}$ : the data subsets utilized for computing the two components of the loss in (5),  $\ell_a$  and  $\ell_u$  respectively. Let  $\mathbf{Z}'$  and  $\mathbf{Z}''$  denote randomly chosen batches of  $\mathcal{D}_1$  and  $\mathcal{D}_2$  at time  $t$ , respectively, while  $\mathbf{U}''$  denotes the corresponding batch of conformity scores  $W_i$  at time  $t$ . The state of Algorithm 1 at time  $t$  is determined by  $\mathbf{U}''$  and  $\zeta^{(t)} = (\mathbf{Z}', \mathbf{Z}'', \theta^{(t)})$ , where  $\theta^{(t)}$  is the vector containing the current values of all weights of the deep neural network. Denote also the gradient of the differentiable approximation  $\tilde{\ell}$  of the loss  $\ell$  in (5) at time  $t$  as  $g^{(t)} = \nabla \tilde{\ell}(\mathbf{Z}', \mathbf{Z}'', \mathbf{U}'')$ .

With this notation in place, one may say the stochastic gradient descent in Algorithm 1 aims to minimize the expectation of  $\tilde{\ell}(\mathbf{Z}', \mathbf{Z}'', \mathbf{U}'') = (1 - \lambda) \cdot \ell_a(\mathbf{Z}') + \lambda \cdot \ell_u(\mathbf{Z}'', \mathbf{U}'')$  conditional on the data  $(X_i, Y_i)_{i \in [n]}$ . Note that  $\tilde{\ell}$  is a deterministic function of  $\mathbf{Z}', \mathbf{Z}'', \mathbf{U}''$  and it is differentiable in  $\theta^{(t)}$ . Define  $J^{(t)}$  as the expected value of  $\tilde{\ell}(\mathbf{Z}', \mathbf{Z}'', \mathbf{U}'')$  conditional on  $\zeta^{(t)}$ :

$$J^{(t)} = \mathbb{E} \left[ \tilde{\ell}(\mathbf{Z}', \mathbf{Z}'', \mathbf{U}'') \mid \zeta^{(t)} \right],$$

where the expectation is taken over the independent uniform random vector  $\mathbf{U}''$ , and let  $\nabla J^{(t)}$  indicate its gradient with respect to  $\theta^{(t)}$ . In practice, at each step Algorithm 1 updates  $\theta^{(t)}$  in the direction of an unbiased estimate  $g^{(t)}$  of  $\nabla J^{(t)}$ , based on an independent random realization of  $\mathbf{U}''$ :

$$g^{(t)} = \nabla \tilde{\ell}(\mathbf{Z}', \mathbf{Z}'', \mathbf{U}''). \quad (\text{A13})$$

This setup makes it possible to prove Algorithm 1 will tend to approach a regime of small  $\nabla J^{(t)}$  after sufficiently many gradient updates, under suitable regularity conditions. This analysis is inspired by [88] and [89], as well as by the approach taken for an analogous convergence result in [90].

**Proposition A3.** Assume there exists a finite Lipschitz constant  $L > 0$  such that, for all parameter configurations  $\theta', \theta''$  and all possible values of the data batches  $\mathbf{Z}', \mathbf{Z}''$ ,

$$\|\nabla \mathbb{E} \left[ \tilde{\ell}(\mathbf{Z}', \mathbf{Z}'', \mathbf{U}'') \mid \mathbf{Z}', \mathbf{Z}'', \theta' \right] - \nabla \mathbb{E} \left[ \tilde{\ell}(\mathbf{Z}', \mathbf{Z}'', \mathbf{U}'') \mid \mathbf{Z}', \mathbf{Z}'', \theta'' \right]\|_2 \leq L \|\theta' - \theta''\|_2. \quad (\text{A14})$$

Assume also the variance of  $g^{(t)}$  in (A13) is uniformly bounded by some  $\sigma^2 \in \mathbb{R}$ :

$$\mathbb{E} \left[ \|g^{(t)} - J^{(t)}\|_2^2 \mid \zeta^{(t)} \right] \leq \sigma^2, \quad \forall t \leq T.$$

Then, for any initial state  $\zeta^{(1)}$  of the learning algorithm and  $\Delta = (2/L) \sup (J^{(1)})$ ,

$$\frac{1}{T} \sum_{t=1}^T \mathbb{E} \left[ \|\nabla J^{(t)}\|_2^2 \mid \zeta^{(1)} \right] \leq \frac{L^2 \Delta}{T} + \left( \mu_0 + \frac{\Delta}{\mu_0} \right) \frac{L\sigma}{\sqrt{T}}.$$

In plain words, Proposition A3 says the squared norm of the gradient of the loss function  $\|\nabla J^{(t)}\|_2^2$  decreases on average at rate  $T^{-1/2}$  as  $T \rightarrow \infty$ . This can be interpreted as a weak form of convergence, although it does not imply that  $\theta^{(t)}$  will reach a global minimum or any other fixed point.

## A2.2 Mathematical proofs

*Proof of Proposition 1.* By definition of the conformity score function  $W(\cdot)$  in (4), for any  $\alpha \in (0, 1)$ ,

$$\begin{aligned} \mathbb{P}[W(X, Y, U; \pi) > 1 - \alpha \mid X = x] &= \mathbb{P}[\min \{t \in [0, 1] : Y \in \mathcal{S}(x, U; \pi, t)\} > 1 - \alpha] \\ &= \mathbb{P}[Y \notin \mathcal{S}(x, U; \pi, 1 - \alpha)] = \alpha. \end{aligned}$$

Above, the second equality follows directly from the fact that  $\mathcal{S}(x, U; \pi, t)$ , defined in (A10), is by construction increasing in  $t$ , and therefore  $Y \notin \mathcal{S}(x, U; \pi, 1 - \alpha)$  if and only if  $\min \{t \in [0, 1] : Y \in \mathcal{S}(x, U; \pi, t)\} > 1 - \alpha$ .  $\square$

*Proof of Proposition 2.* The proof consists of showing that  $\ell_a$  and  $\ell_u$  are separately minimized by  $\hat{\pi} = \pi$ , although only approximately in the latter case. Without loss of generality, we will assume that  $\mathcal{I}_1 = \mathcal{I}_2 = M = n/2$ , to simplify the notation.

The first part of the proof is standard and proceeds as follows. Recall that the cross entropy loss  $\ell_a$  defined in (6) is

$$\ell_a = -\frac{1}{M} \sum_{i \in \mathcal{I}_1} \sum_{c=1}^K Y_{i,c} \log \hat{\pi}_c(X_i),$$

where  $Y_{i,c} = \mathbb{1}[Y_i = c]$  and  $\hat{\pi}_c(X_i) = \hat{\mathbb{P}}[Y_i = c \mid X = x]$ . Then, the expected value of  $\ell_a$ , taken over the randomness in the data indexed by  $\mathcal{I}_1$ , is

$$\begin{aligned} \mathbb{E}[\ell_a] &= -\frac{1}{M} \sum_{i \in \mathcal{I}_1} \sum_{c=1}^K \mathbb{E}[Y_{i,c} \log \hat{\pi}_c(X_i)] \\ &= -\frac{1}{M} \sum_{i \in \mathcal{I}_1} \sum_{c=1}^K \mathbb{E}[\mathbb{E}[Y_{i,c} \log \hat{\pi}_c(X_i) \mid X_i]] \\ &= -\frac{1}{M} \sum_{i \in \mathcal{I}_1} \sum_{c=1}^K \mathbb{E}[\mathbb{E}[Y_{i,c} \mid X_i] \log \hat{\pi}_c(X_i)] \\ &= -\frac{1}{M} \sum_{i \in \mathcal{I}_1} \mathbb{E} \left[ \sum_{c=1}^K \pi_c(X_i) \log \hat{\pi}_c(X_i) \right] \\ &= \frac{1}{M} \sum_{i \in \mathcal{I}_1} \mathbb{E}[H(\pi(X_i), \hat{\pi}(X_i))] \\ &= \mathbb{E}[H(\pi(X), \hat{\pi}(X))], \end{aligned}$$

where  $H(\pi(X), \hat{\pi}(X))$  is the cross entropy of the conditional distribution  $\hat{\pi}$  relative to the conditional distribution  $\pi$  given  $X$ . Note that the last equality above simply follows from the underlying assumption that the data consist of i.i.d. observations from some unknown distribution  $P_{XY}$ .

This implies that  $\mathbb{E}[\ell_a]$  is minimized by  $\hat{\pi} = \pi$ , because the cross entropy can be written as

$$H(\pi(X), \hat{\pi}(X)) = H(\pi(X)) + D_{KL}(\pi(X) \parallel \hat{\pi}(X)),$$

where  $H(\pi(X))$  is the (constant) entropy of  $\pi(X)$  and  $D_{KL}$  denotes the Kullback–Leibler divergence, which is always non-negative and exactly equal to 0 if  $\hat{\pi} = \pi$ .

For the second part of the proof, recall that  $\ell_u$  was defined in (7) as:

$$\ell_u = \mathcal{K}(\mathbf{W}),$$

where  $\mathbf{W} \in \mathbb{R}^M$  are the conformity scores on  $\mathcal{I}_2$ , and  $\mathcal{K}$  is the Kolmogorov–Smirnov distance from the uniform distribution:

$$\mathcal{K}(\mathbf{W}) = \sup_{w \in [0,1]} \left| \hat{F}_M(w) - w \right|.$$

Above,  $\hat{F}_M$  is the empirical CDF of the scores. Note that  $\mathcal{K}(\mathbf{W})$  can be bound from above by

$$\begin{aligned} \mathcal{K}(\mathbf{W}) &= \sup_{w \in [0,1]} \left| \hat{F}_M(w) - w \right| \\ &= \sup_{w \in [0,1]} \left| \hat{F}_M(w) - F(w) + F(w) - w \right| \\ &\leq \sup_{w \in [0,1]} \left| \hat{F}_M(w) - F(w) \right| + \sup_{w \in [0,1]} |F(w) - w|, \end{aligned}$$

where  $F$  is the true CDF of the conformity scores and the last step above is the triangle inequality. The first term on the right-hand-side above can be bound by the DKW inequality [91]:

$$\mathbb{P} \left[ \sup_{w \in [0,1]} \left| \hat{F}_M(w) - F(w) \right| \geq \epsilon \right] \leq 2 \exp^{-2M\epsilon^2}, \quad \forall \epsilon > 0.$$

Therefore, we have obtained that

$$\ell_u \leq \sup_{w \in [0,1]} |F(w) - w| + \mathcal{O}_{\mathbb{P}} \left( \frac{1}{\sqrt{M}} \right).$$

According to Proposition 1, the conformity scores follow a uniform distribution if  $\hat{\pi} = \pi$ , and therefore in that case  $\sup_{w \in [0,1]} |F(w) - w| = 0$ . This completes the proof.  $\square$

*Proof of Proposition A3.* The proof is essentially the same as that of Supplemental Theorem S1 in [90], but we nonetheless report here all details here completeness. First, note that a first-order Taylor expansion applied to the gradient update of Algorithm 1 yields

$$J^{(t+1)} \leq J^{(t)} + \langle \nabla J^{(t)}, \theta^{(t+1)} - \theta^{(t)} \rangle + \frac{L}{2} \mu^2 \|g^{(t)}\|_2^2.$$

Define  $\delta^{(t)} = g^{(t)} - \nabla J^{(t)}$ . Then, as  $-\mu g^{(t)} = \theta^{(t+1)} - \theta^{(t)}$ , the above inequality can be written as

$$\begin{aligned} J^{(t+1)} &\leq J^{(t)} - \mu \langle \nabla J^{(t)}, g_t \rangle + \frac{L}{2} \mu^2 \|g^{(t)}\|_2^2 \\ &= J^{(t)} - \mu \|\nabla J^{(t)}\|_2^2 - \mu \langle \nabla J^{(t)}, \delta_t \rangle + \frac{L}{2} \mu^2 \left( \|\nabla J^{(t)}\|_2^2 + 2 \langle \nabla J^{(t)}, \delta_t \rangle + \|\delta_t\|_2^2 \right) \\ &= J^{(t)} - \left( \mu - \frac{L}{2} \mu^2 \right) \|\nabla J^{(t)}\|_2^2 - (\mu - L\mu^2) \langle \nabla J^{(t)}, \delta_t \rangle + \frac{L}{2} \mu^2 \|\delta^{(t)}\|_2^2. \end{aligned}$$

Summing the above inequalities over  $t = 1, \dots, T$ , and noting that  $J^{(t)} \geq 0$  for all  $t$ , we obtain:

$$\begin{aligned} \left( \mu - \frac{L}{2} \mu^2 \right) \sum_{t=1}^T \|\nabla J^{(t)}\|_2^2 &\leq J^{(1)} - J^{(t+1)} - (\mu - L\mu^2) \sum_{t=1}^T \langle \nabla J^{(t)}, \delta^{(t)} \rangle + \frac{\mu^2 L}{2} \sum_{t=1}^T \|\delta^{(t)}\|_2^2 \\ &\leq J^{(1)} - (\mu - L\mu^2) \sum_{t=1}^T \langle \nabla J^{(t)}, \delta^{(t)} \rangle + \frac{\mu^2 L}{2} \sum_{t=1}^T \|\delta^{(t)}\|_2^2. \end{aligned} \tag{A15}$$

Recall that the estimated gradients  $g^{(t)}$  are unbiased, i.e.  $\mathbb{E}[g^{(t)} | \zeta^{(t)}] = \nabla J^{(t)}$ . Therefore, taking the conditional expectation of both sides of (A15) given  $\zeta^{(1)}$  leads to

$$\begin{aligned}\mathbb{E}[\langle \nabla J^{(t)}, \delta^{(t)} \rangle | \zeta^{(1)}] &= \mathbb{E}[\mathbb{E}[\langle \nabla J^{(t)}, \delta^{(t)} \rangle | \zeta^{(1)}, \zeta^{(t)}] | \zeta^{(1)}] \\ &= \mathbb{E}[\mathbb{E}[\langle \nabla J^{(t)}, \delta^{(t)} \rangle | \zeta^{(t)}] | \zeta^{(1)}] \\ &= \mathbb{E}[\langle \nabla J^{(t)}, \mathbb{E}[\delta^{(t)} | \zeta^{(t)}] \rangle | \zeta^{(1)}] \\ &= \mathbb{E}[\langle \nabla J^{(t)}, 0 \rangle | \zeta^{(1)}] = 0.\end{aligned}$$

Replacing this result into (A15), and leveraging the assumption that  $\mathbb{E}[\|\delta^{(t)}\|_2^2 | \zeta^{(t)}] \leq \sigma^2$ , leads to

$$\left(\mu - \frac{L}{2}\mu^2\right) \sum_{t=1}^T \mathbb{E}[\|\nabla J^{(t)}\|_2^2 | \zeta^{(1)}] \leq J^{(1)} + \frac{\mu^2 L}{2} T \sigma^2.$$

Then, multiplying both sides above by  $2/[LT(2\mu - L\mu^2)]$  results in

$$\frac{1}{TL} \sum_{t=1}^T \mathbb{E}[\|\nabla J^{(t)}\|_2^2 | \zeta^{(1)}] \leq \frac{2J^{(1)}}{TL(2\mu - L\mu^2)} + \frac{\sigma^2 \mu}{2 - L\mu} \leq \frac{\Delta}{T(2\mu - L\mu^2)} + \frac{\sigma^2 \mu}{2 - L\mu}.$$

Finally, choosing  $\mu = \min\left\{\frac{1}{L}, \frac{\mu_0}{\sigma\sqrt{T}}\right\}$  for some  $\mu_0 > 0$  gives the desired result:

$$\frac{1}{T} \sum_{t=1}^T \mathbb{E}[\|\nabla J^{(t)}\|_2^2 | \zeta^{(1)}] \leq \frac{L^2 \Delta}{T} + \left(\mu_0 + \frac{\Delta}{\mu_0}\right) \frac{L\sigma}{\sqrt{T}}.$$

□

## A3 Additional details and results from numerical experiments

### A3.1 Details about experiments with synthetic data

The conditional data-generating distribution of  $Y$  given  $X$  is given by:

$$\mathbb{P}[Y | X] = \begin{cases} \left(\frac{1}{K/2}, \frac{1}{K/2}, \frac{1}{K/2}, 0, 0, 0\right), & \text{if } X_1 \leq \delta, X_2 < 0.5, \\ \left(0, 0, 0, \frac{1}{K/2}, \frac{1}{K/2}, \frac{1}{K/2}\right), & \text{if } X_1 \leq \delta, X_2 \geq 0.5, \\ (1, 0, 0, 0, 0, 0), & \text{if } X_1 > \delta, 0 \leq X_3 \leq \frac{1}{K}, \\ (0, 1, 0, 0, 0, 0), & \text{if } X_1 > \delta, \frac{1}{K} \leq X_3 \leq \frac{2}{K}, \\ \vdots & \vdots \\ (0, 0, 0, 0, 0, 1), & \text{if } X_1 > \delta, \frac{K-1}{K} \leq X_3 \leq 1, \end{cases} \quad (\text{A16})$$

Above, we set  $\delta = 0.2$ , so that 20% of the samples are impossible to classify with absolute confidence.

The model trained to predict  $Y | X$  is a fully connected neural network implemented in PyTorch [79], with 5 layers of width 256, 256, 128 and 64 and ReLU activations; the conditional class probabilities  $\hat{\pi}$  are output by a final softmax layer. For both our new method and the hybrid method, the batch size is 750 and the hyper-parameter  $\lambda$  controlling the relative weights of the two components of the loss is 0.2. Our method (resp., the hybrid method) is applied using 5/6 of the data to evaluate the cross entropy and 1/6 for the conformity score (resp., conformal size) loss. The models minimizing the cross entropy and focal loss are trained via stochastic gradient descent for 3000 epochs with batch size 200 and initial learning rate 0.01, decreased by a factor 10 halfway through training; see below for details about early stopping. The hybrid loss model is trained via stochastic gradient descent for 4000 epochs with learning rate 0.01 decreased by a factor 10 halfway through training. The conformal uncertainty-aware model is trained via Adam [92] for 4000 epochs with learning rate 0.001 decreased by a factor 10 halfway through training.

### A3.2 Results with synthetic data

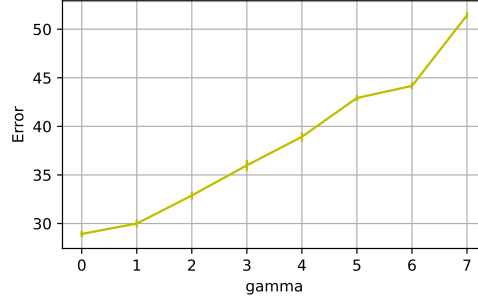


Figure A5: Best-guess misclassification rate on test data for a deep classifier trained to minimize the focal loss, with early stopping based on validation prediction accuracy. The results are averaged over 50 independent experiments and shown as a function of the loss function hyper-parameter  $\gamma$ . The size of the training sample is 2400. Other details are as in Figure 1.

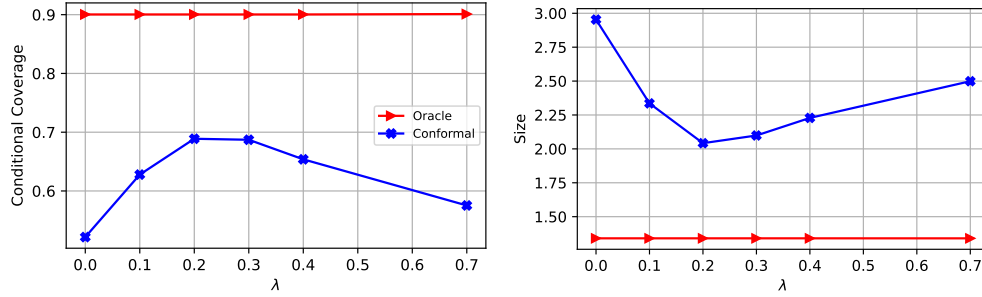


Figure A6: Conditional coverage (left) and average size (right) of conformal prediction sets obtained with our method in the numerical experiments with synthetic data of Figure 1, compared to the ideal results produced by a perfect oracle. Early stopping based on validation accuracy is employed. The results are shown as a function of the hyper-parameter  $\lambda$  in (5). The number of training data points is 2400.

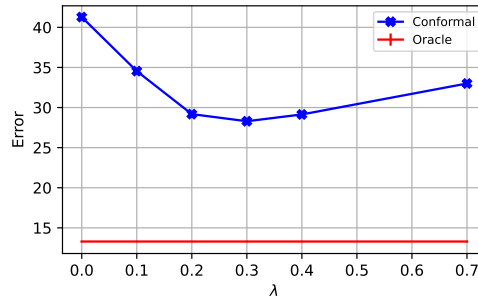


Figure A7: Average accuracy of best-guess predictions computed by models trained with our method in the numerical experiments with synthetic data of Figure 1, compared to the ideal results produced by a perfect oracle. Early stopping based on validation accuracy is employed. Other details are as in Figure A6.

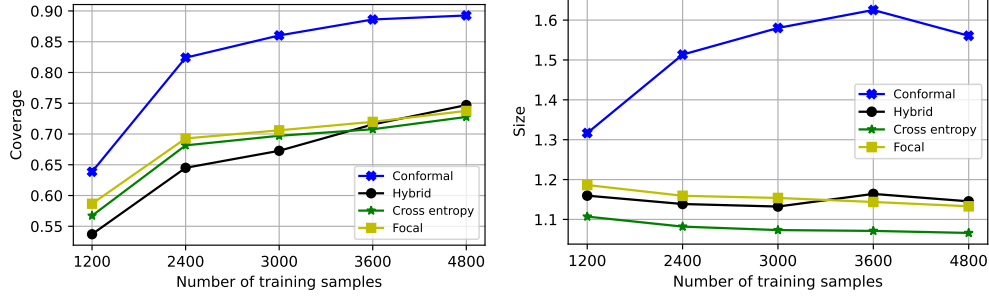


Figure A8: Marginal coverage (left) and average size (right) of conformal prediction sets obtained with different learning method in the numerical experiments of Figure 1, without post-training conformal calibration. The nominal target level is 90%. Other details are as in Figure 1.

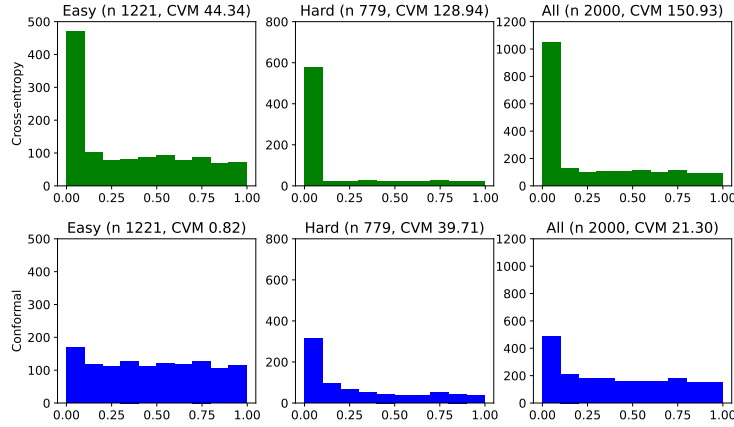


Figure A9: Histograms of conformity scores on synthetic test data obtained with deep classification models trained to minimize the cross entropy (top) or the proposed proposed conformal loss (bottom). The scores are shown separately based on the intrinsic difficulty of the test samples. Left: samples with  $X_1 > 0.2$  (easy). Center: samples with  $X_1 \leq 0.2$  (hard). Right: all samples. These test data contain approximately 40% of hard samples. The numbers displayed after the “CVM” acronym are the values of the Cramer von Mises [75, 76] statistic for testing the uniformity in distribution of the conformity scores; smaller values indicate a more uniform distribution. Other details are as in Figure 1.



Figure A10: Histograms of conditional class probabilities ( $\mathbb{P}[Y = 2 \mid X]$ ) computed on test synthetic data by the true oracle model (top) or estimated by a deep classification network minimizing the cross entropy (middle) or the proposed conformal loss (bottom). Other details are as in Figure A9.

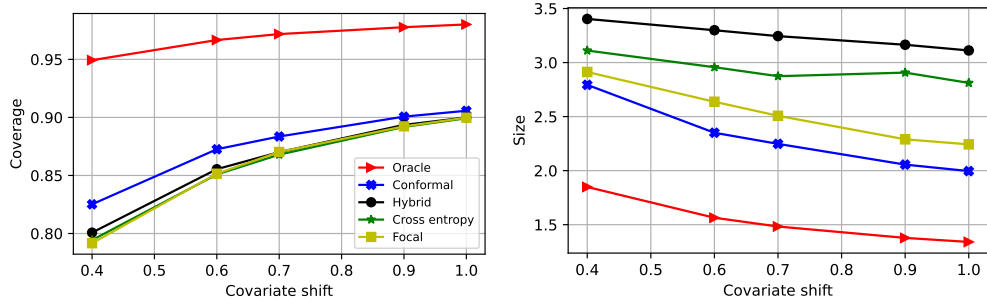


Figure A11: Performance of conformal prediction sets with 90% marginal coverage based on the ideal oracle model and a deep neural network trained with four alternative algorithms. The models are fully trained with 2400 samples, and the results are shown as a function of the amount of covariate shift. Covariate shift=1 corresponds to no covariate shift (20% of hard-to-classify samples), while lower values of covariate shift correspond to test sets with more numerous hard-to-classify samples compared to the training and calibration data sets. Other details are as in Figure 1.

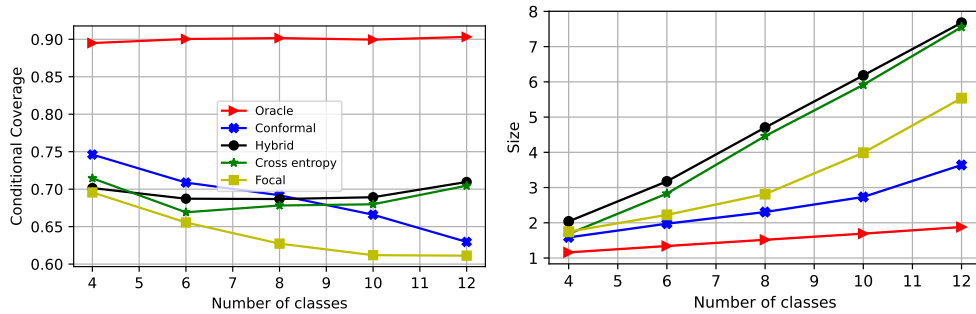


Figure A12: Performance of conformal prediction sets with 90% marginal coverage based on the ideal oracle model and a deep neural network trained with four alternative algorithms. The models are fully trained with 2400 samples, and the results are shown as a function of the number  $K$  of possible classes. Other details are as in Figure 1.

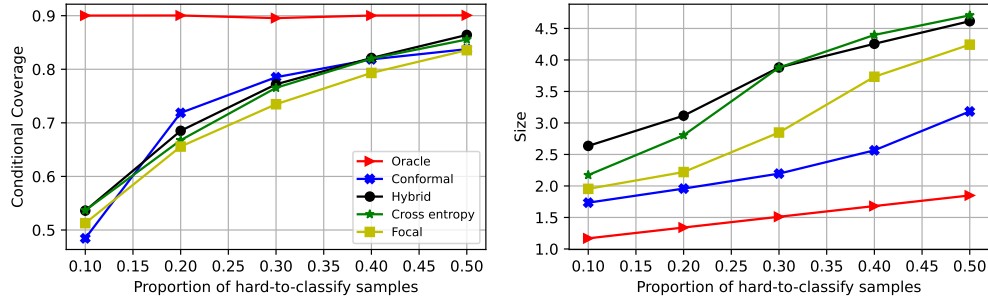


Figure A13: Performance of conformal prediction sets with 90% marginal coverage based on the ideal oracle model and a deep neural network trained with four alternative algorithms. The models are fully trained with 2400 samples, and the results are shown as a function of the proportion  $\delta$  of hard-to-classify samples in the data. Other details are as in Figure 1.

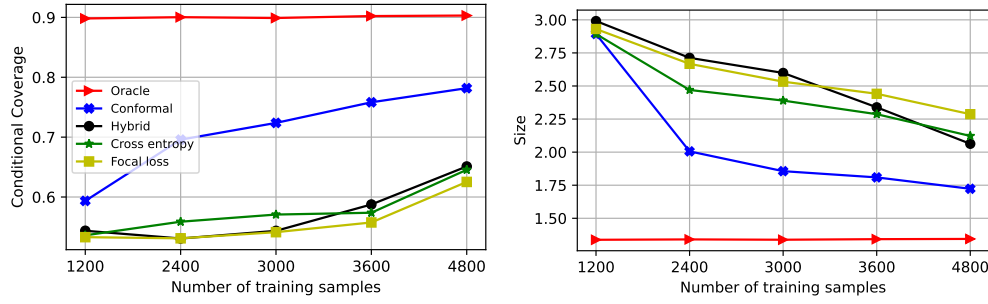


Figure A14: Performance of conformal prediction sets with 90% marginal coverage based on the oracle model and a deep neural network trained with different algorithms. The models are trained with 2400 samples and early stopping based on maximum accuracy on validation data. Other details are as in Figure 1.

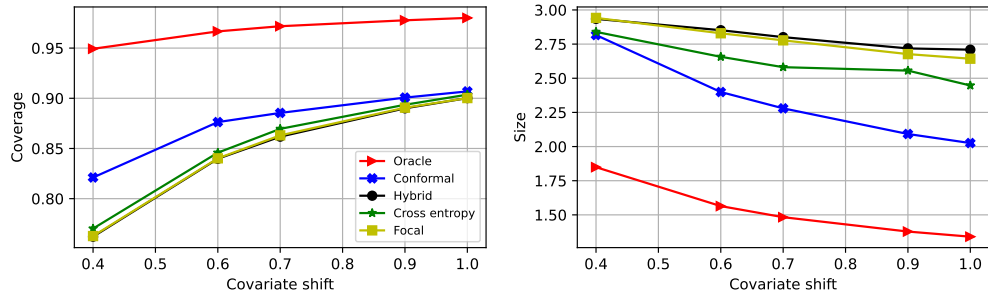


Figure A15: Performance of conformal prediction sets with 90% marginal coverage based on the ideal oracle model and a deep neural network trained with four alternative algorithms using 2400 training samples. The results are shown as a function of the amount of covariate shift. Early stopping based on validation accuracy is employed. Other details are as in Figure A11.

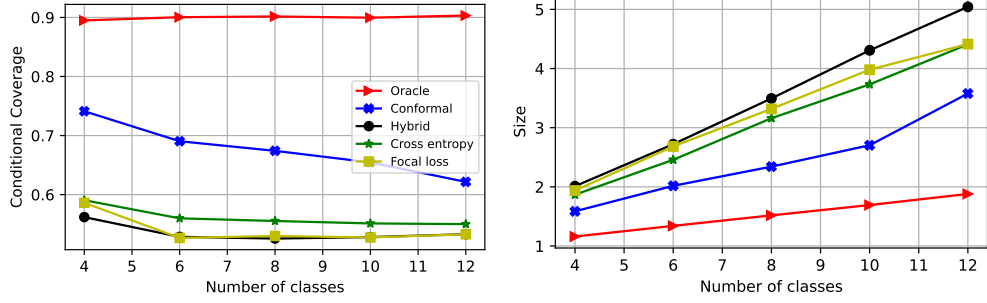


Figure A16: Performance of conformal prediction sets with 90% marginal coverage based on the oracle model and a deep neural network trained with different algorithms. The models are trained with 2400 samples and early stopping based on maximum accuracy on validation data. Other details are as in Figure A12.

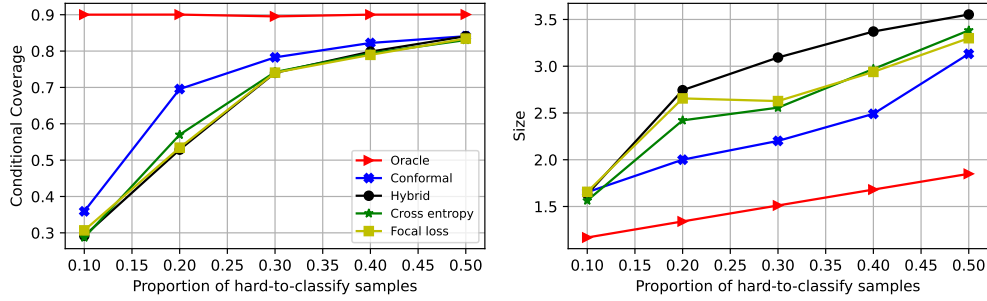


Figure A17: Performance of conformal prediction sets with 90% marginal coverage based on the oracle model and a deep neural network trained with different algorithms. The models are trained with 2400 samples and early stopping based on maximum accuracy on validation data. Other details are as in Figure A13.

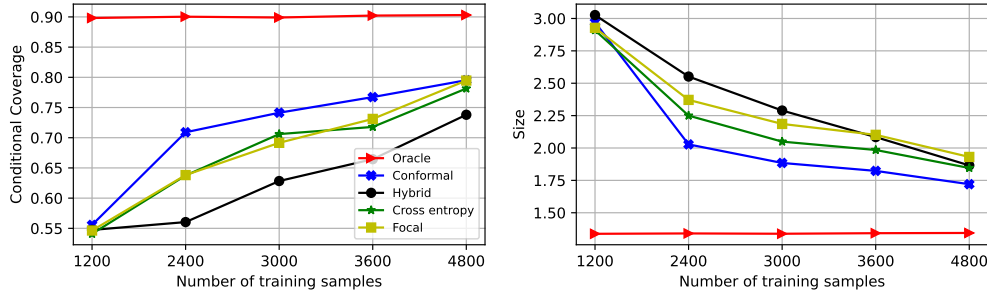


Figure A18: Performance of conformal prediction sets with 90% marginal coverage based on the oracle model and a deep neural network trained with different algorithms. The models are trained with 2400 samples and early stopping based on minimum validation loss. Other details are as in Figure 1.

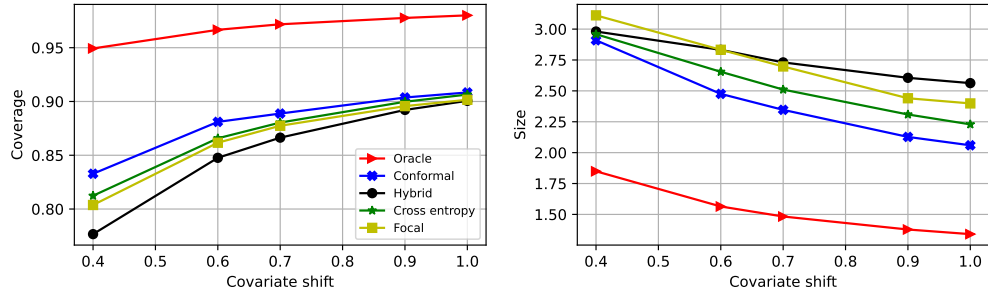


Figure A19: Performance of conformal prediction sets with 90% marginal coverage based on the ideal oracle model and a deep neural network trained with four alternative algorithms using 2400 training samples. The results are shown as a function of the amount of covariate shift. Early stopping based on minimum validation loss is employed. Other details are as in Figure A11.

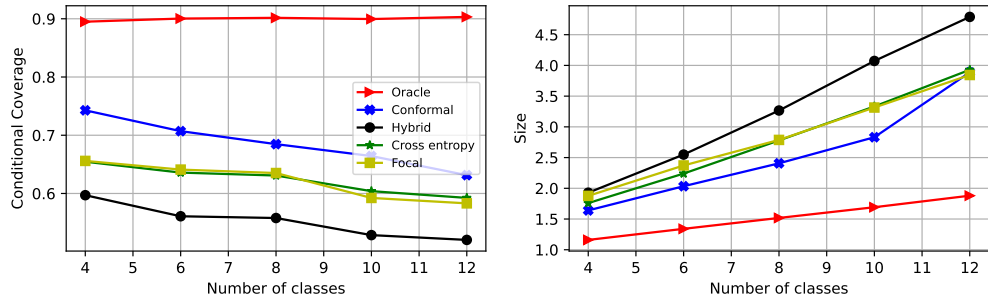


Figure A20: Performance of conformal prediction sets with 90% marginal coverage based on the oracle model and a deep neural network trained with different algorithms. The models are trained with 2400 samples and early stopping based on minimum validation loss. Other details are as in Figure A12.

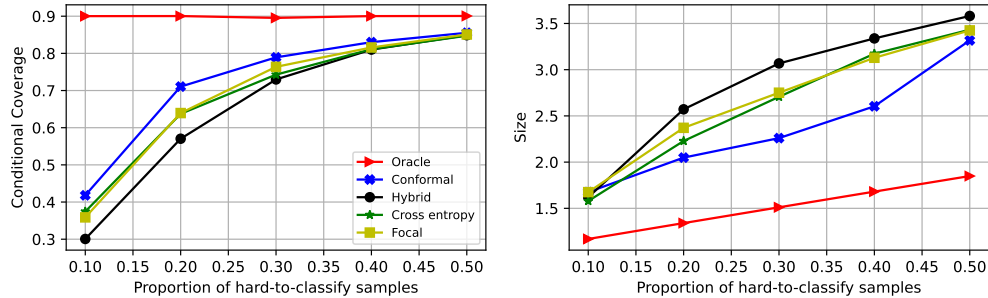


Figure A21: Performance of conformal prediction sets with 90% marginal coverage based on the oracle model and a deep neural network trained with different algorithms. The models are trained with 2400 samples and early stopping based on minimum validation loss. Other details are as in Figure A13.

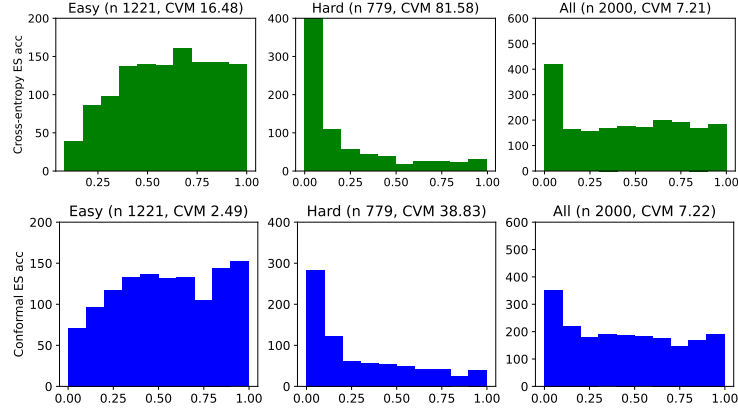


Figure A22: Histograms of conformity scores on synthetic test data obtained with deep classification models trained to minimize different losses. The models are trained with early stopping based on maximum validation accuracy. Other details are as in Figure A9.

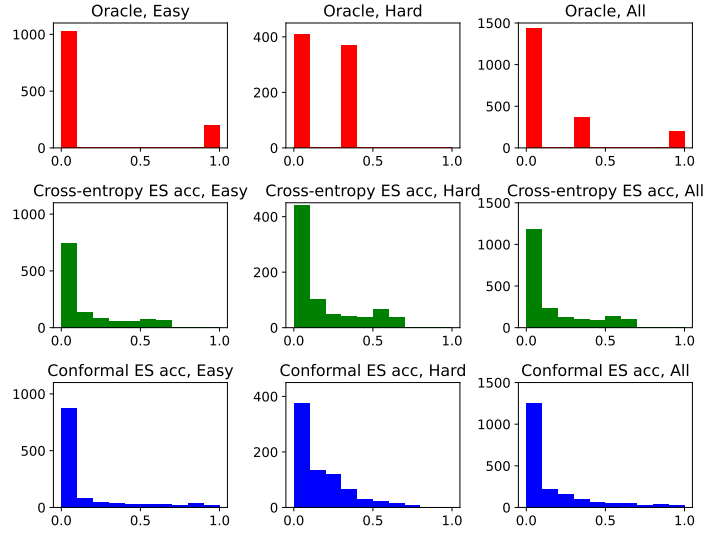


Figure A23: Histograms of conditional class probabilities ( $\mathbb{P}[Y = 2 | X]$ ) computed on test synthetic data by the true oracle model or estimated by a deep classification network minimizing different loss functions. The models are trained with early stopping based on maximum validation accuracy. Other details are as in Figure A10.

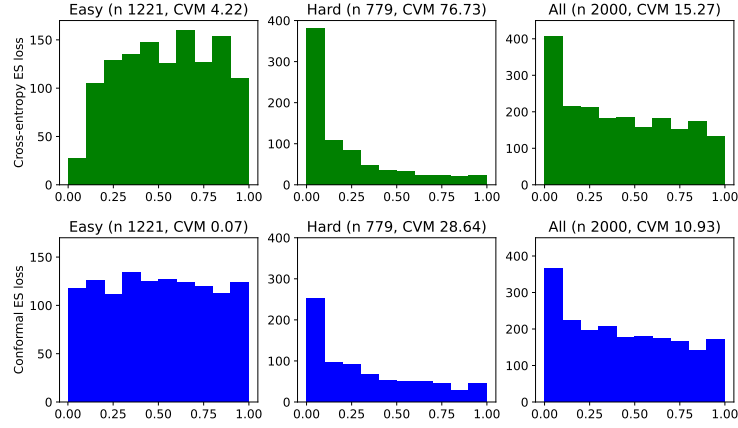


Figure A24: Histograms of conformity scores on synthetic test data obtained with deep classification models trained to minimize different losses. The models are trained with early stopping based on minimum validation loss. Other details are as in Figure A9.

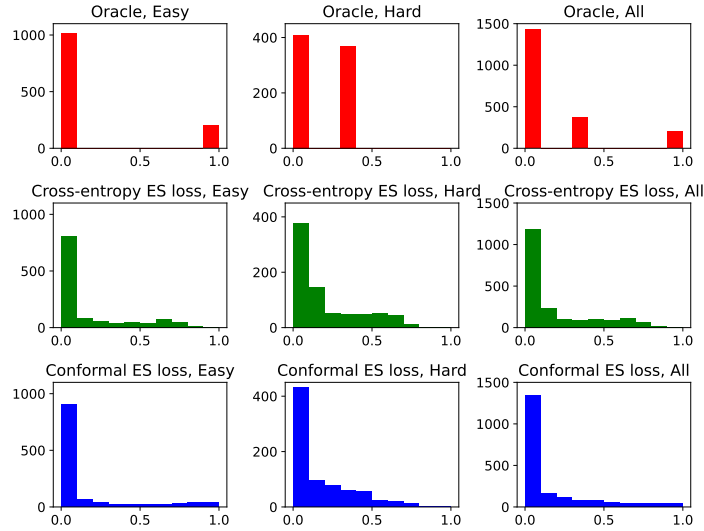


Figure A25: Histograms of conditional class probabilities ( $\mathbb{P}[Y = 2 | X]$ ) computed on test synthetic data by the true oracle model or estimated by a deep classification network minimizing different loss functions. The models are trained with early stopping based on minimum validation loss. Other details are as in Figure A10.

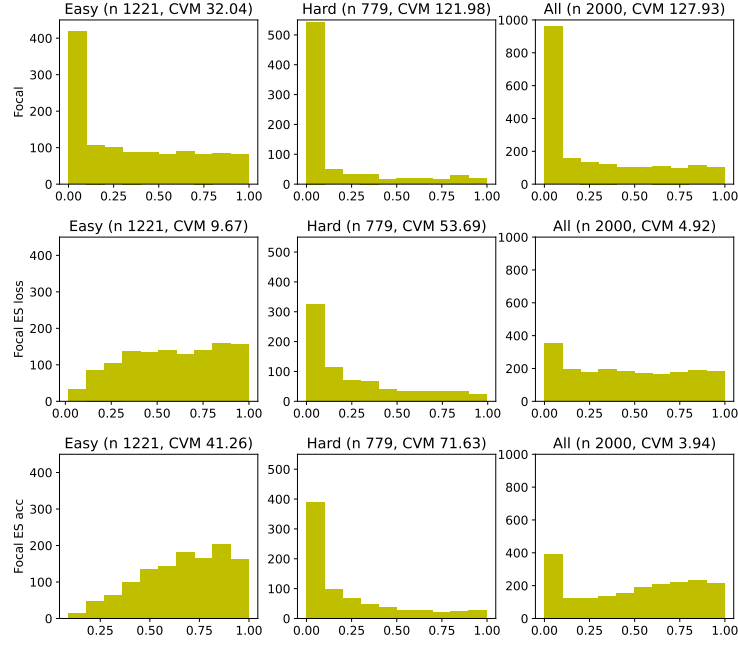


Figure A26: Histograms of conformity scores on synthetic test data obtained with deep classification models trained to minimize the focal loss. Top: fully trained model. Center: early stopping (ES) based on minimum validation loss (ES loss). Bottom: early stopping based on maximum validation accuracy (ES acc). Other details are as in Figure A9.

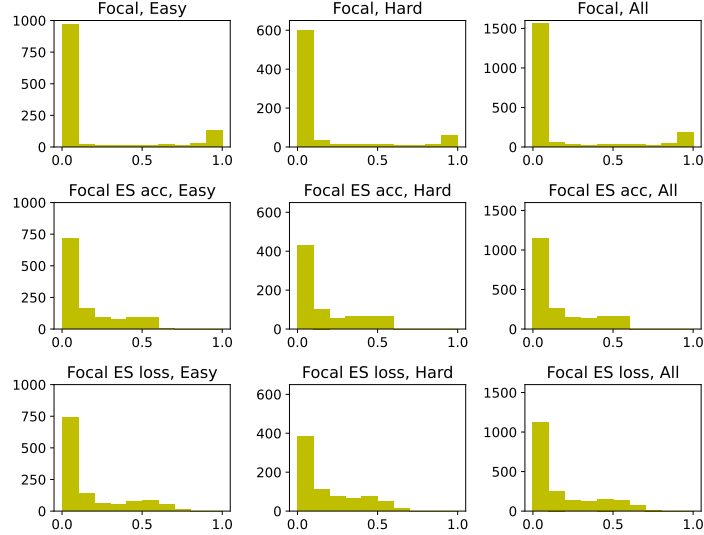


Figure A27: Histograms of conditional class probabilities ( $\mathbb{P}[Y = 2 | X]$ ) computed on test synthetic data by a deep classification network minimizing the focal loss. Top: fully trained model. Center: early stopping based on minimum validation loss. Bottom: early stopping based on maximum validation accuracy. Other details are as in Figure A10.

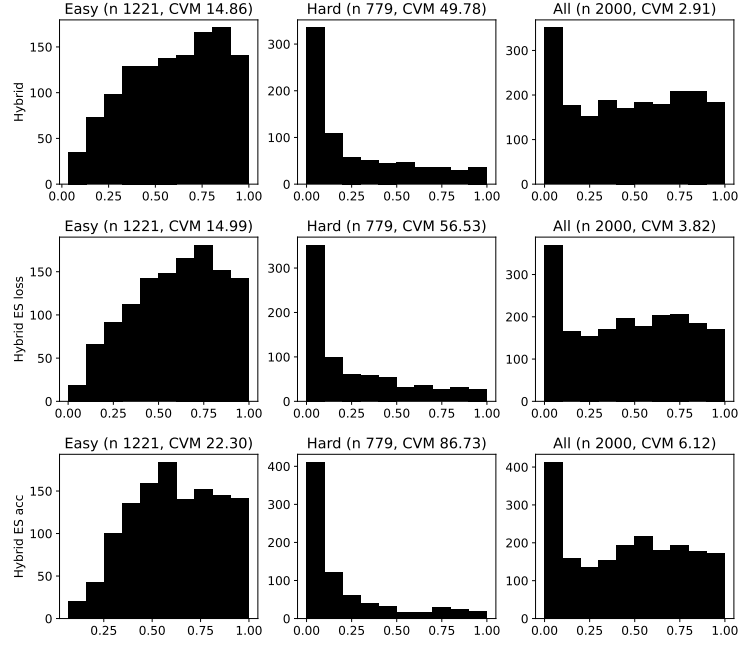


Figure A28: Histograms of conformity scores on synthetic test data obtained with deep classification models trained to minimize the hybrid loss. Top: fully trained model. Center: early stopping based on minimum validation loss. Bottom: early stopping based on maximum validation accuracy. Other details are as in Figure A9.

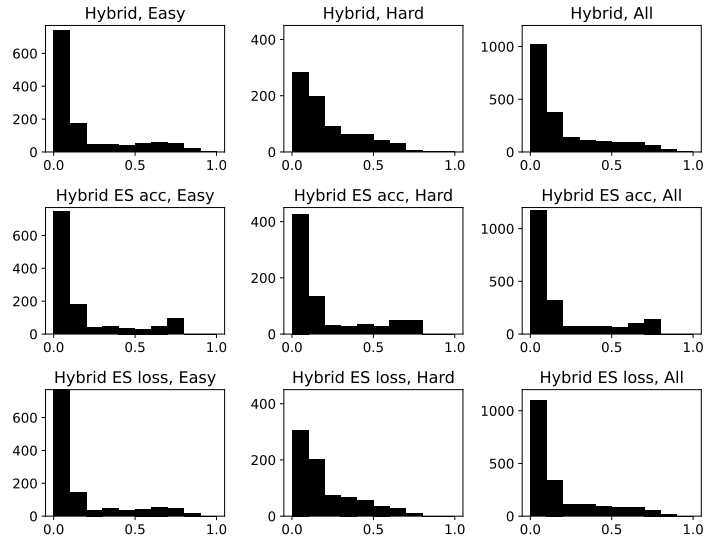


Figure A29: Histograms of conditional class probabilities ( $\mathbb{P}[Y = 2 | X]$ ) computed on test synthetic data by a deep classification network minimizing the hybrid loss. Top: fully trained model. Center: early stopping based on minimum validation loss. Bottom: early stopping based on maximum validation accuracy. Other details are as in Figure A10.

### A3.3 Details about experiments with CIFAR-10 data

All images undergo standard normalization pre-processing. Then, the RandomErasing [82] method implemented in PyTorch [79] is applied with scale parameter 0.8 and ratio 0.3, and the fraction of corrupted images is varied within  $\{0.01, 0.025, 0.05, 0.1, 0.2\}$ . All models are trained on  $\{3000, 10000, 16500, 27500, 45000\}$  samples. A ResNet-18 architecture for Cifar-10 is utilized, after modifying the original ResNet-18 network for ImageNet [93] as in <https://github.com/kuangliu/pytorch-cifar>: the kernel size of the first convolution layer is changed to 3x3, striding is removed, and the first maxpool operation is omitted. For the *conformal loss*, the hyper-parameter  $\lambda$  controlling the relative weights of the uniform matching and cross entropy components is set to be 0.1. Then, the loss is approximately minimized using the Adam optimizer and a batch size of 768. The learning rate is initialized to 0.001 and then decreased by a factor 10 halfway through the training. The number of epochs is 2000 when training with 45000 samples; this is increased to 3200, 3500, 4000, and 5000 when training with 27500, 16500, 10000, and 3000 samples, respectively, as to reach a reasonably stationary state in each case. For the *cross entropy* loss, which is equivalent to the above loss with  $\lambda = 0$ , the batch size is 128 and the optimizer is stochastic gradient descent, which we have observed to work better in this case. The number of epochs is 1000 in the case of largest samples size, and 1500 with smaller samples. The learning rate is initialized to 0.1 and then decreased by a factor 10 halfway through the training. For the *focal loss*, we follow [80] and utilize stochastic gradient descent with batches of size 128. The main focal loss hyper-parameter is set equal to 3. The number of epochs is 1000 with 45000 samples, and similarly to the case of the cross entropy, it is increased to 1500 for smaller sample sizes. The learning rate is initialized to 0.1 and then decreased by a factor 10 halfway through the training. For the *hybrid loss*, the size hyper-parameter is set equal to 0.2. The optimizer is Adam with batch size 768. The number of epochs is 3000 with 45000 samples, and 3500, 3800, 5000, and 5000 when training with 27500, 16500, 10000, and 3000 samples, respectively. The learning rate is initialized to 0.001 and then decreased by a factor 10 halfway through the training. These hyper-parameters were tuned to separately maximize the performance of each method.

### A3.4 Results with CIFAR-10 data

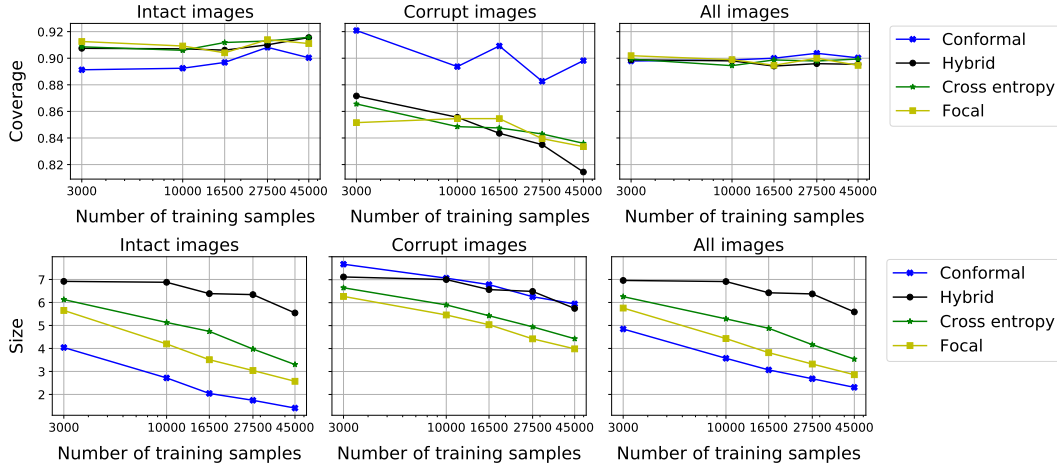


Figure A30: Performance of conformal prediction sets with 90% marginal coverage on CIFAR-10 data, based on convolutional neural networks trained with different loss functions. Top: conditional coverage based, separately for intact and corrupt images. Bottom: size of the prediction sets. The proportion of corrupted images in the training data is 20%

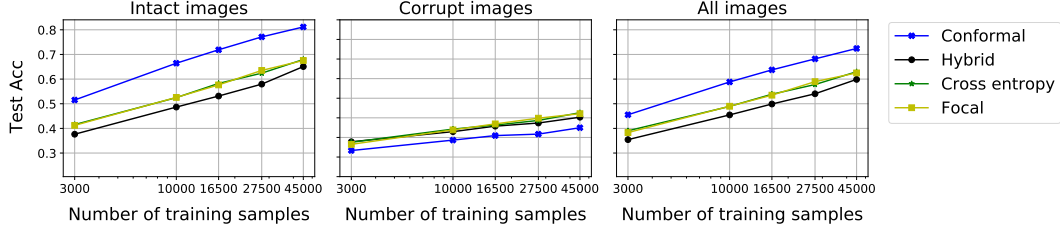


Figure A31: Test accuracy (Acc) of classification models trained on CIFAR-10 data, based on convolutional neural networks trained with different loss functions. Other details are as in Figure 1.

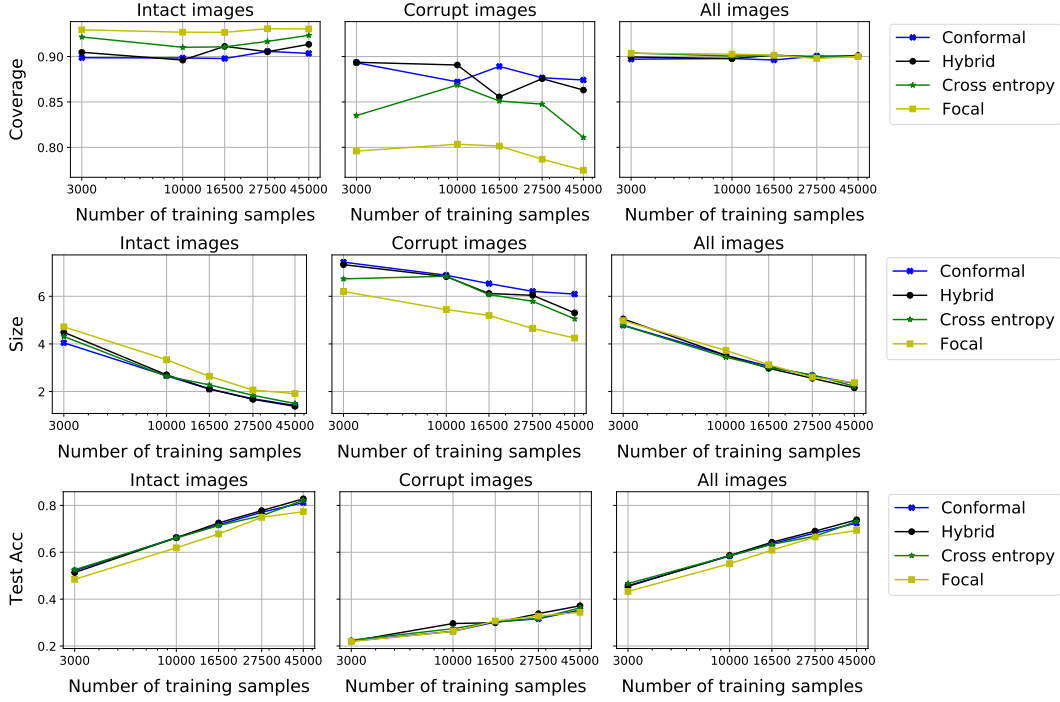


Figure A32: Performance of conformal prediction sets with 90% marginal coverage on CIFAR-10 data, based on convolutional neural networks trained with different loss functions. The models are trained with early stopping based on validation classification accuracy. Top: conditional coverage, separately for intact and corrupt images. Middle: size of the prediction sets. Bottom: test accuracy. Other details are as in Figure A30.

	Coverage intact/corrupted			Size intact/corrupted			Accuracy intact/corrupted		
	Full	ES (acc)	ES (loss)	Full	ES (acc)	ES (loss)	Full	ES (acc)	ES (loss)
Conformal	0.90/0.90	0.90/0.87	0.94/0.79	1.41/5.95	1.41/6.09	1.86/5.12	0.81/0.35	0.81/0.35	0.79/0.29
Hybrid	0.92/0.81	0.91/0.86	0.92/0.83	5.54/5.75	1.38/5.30	1.67/5.37	0.65/0.40	0.83/0.37	0.80/0.32
Cross Entropy	0.92/0.84	0.92/0.81	0.92/0.82	3.30/4.43	1.50/5.05	1.51/4.95	0.68/0.43	0.82/0.36	0.82/0.36
Focal	0.91/0.83	0.93/0.77	0.94/0.81	2.57/3.99	1.91/4.25	2.08/4.58	0.68/0.42	0.77/0.34	0.76/0.35

Table A3: Performance of conformal prediction sets with 90% marginal coverage on CIFAR-10 data, based on models trained on 45,000 data points. The models are either trained fully for many epochs, or trained with early stopping (ES) based on different criteria: highest classification accuracy (acc) or lowest loss (loss). Other details are as in Table 1.

	Coverage intact/corrupted			Size intact/corrupted			Accuracy intact/corrupted		
	Full	ES (acc)	ES (loss)	Full	ES (acc)	ES (loss)	Full	ES (acc)	ES (loss)
Conformal	0.89/0.92	0.90/0.89	0.93/0.78	4.04/7.67	4.05/7.43	4.49/6.31	0.52/0.23	0.52/0.22	0.50/0.20
Hybrid	0.91/0.87	0.90/0.89	0.95/0.72	6.92/7.12	4.49/7.33	5.4/5.96	0.38/0.28	0.51/0.22	0.46/0.17
Cross Entropy	0.91/0.87	0.92/0.84	0.95/0.71	6.13/6.65	4.31/6.73	5.24/5.73	0.42/0.28	0.53/0.23	0.44/0.17
Focal	0.91/0.85	0.93/0.80	0.96/0.70	5.65/6.27	4.72/6.20	5.61/5.77	0.41/0.26	0.48/0.22	0.44/0.18

Table A4: Performance of conformal prediction sets with 90% marginal coverage on CIFAR-10 data, based on models trained on 3,000 data points. Other details are as in Table A3.

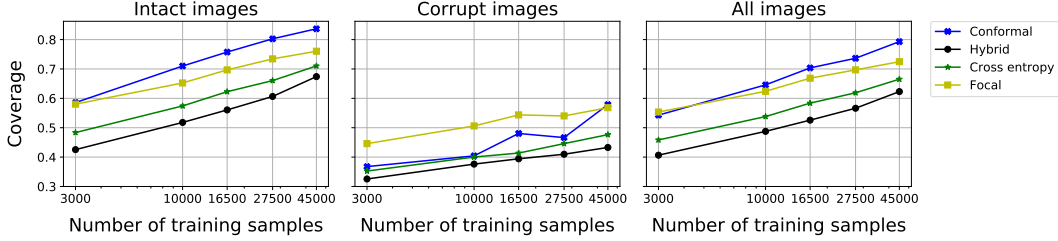


Figure A33: Marginal coverage of conformal prediction sets obtained with different learning method in the numerical experiments of Figure A30, without post-training conformal calibration. The target coverage level is 90%. Other details are as in Figure A30.

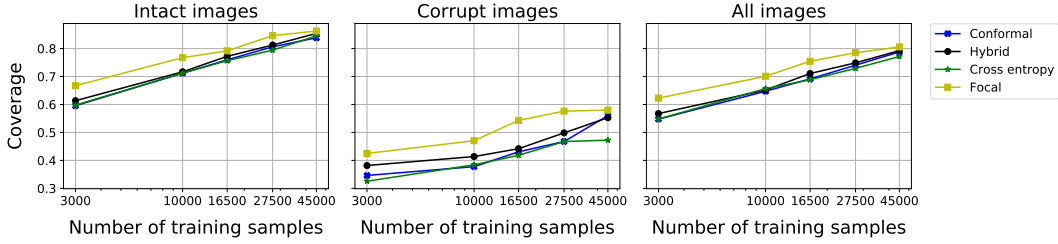


Figure A34: Marginal coverage of conformal prediction sets obtained with different learning method in the numerical experiments of Figure A32, without post-training conformal calibration. The target coverage level is 90%. Other details are as in Figure A32.

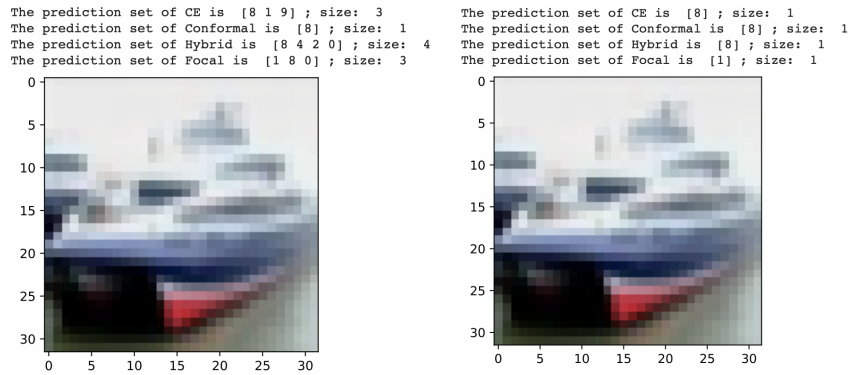


Figure A35: Examples of prediction sets for an intact image, based on models fully trained with different methods, with (left) and without (right) post-training conformal calibration. These experiments are based on the CIFAR-10 data utilized in Table 1. The nominal coverage level is 0.9.

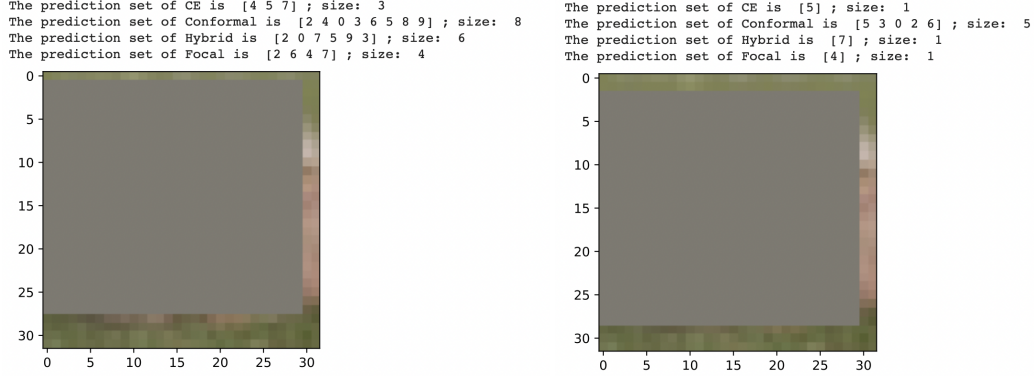


Figure A36: Examples of prediction sets for a corrupt image, based on models fully trained with different methods, with (left) and without (right) post-training conformal calibration. Other details are as in Figure A35.

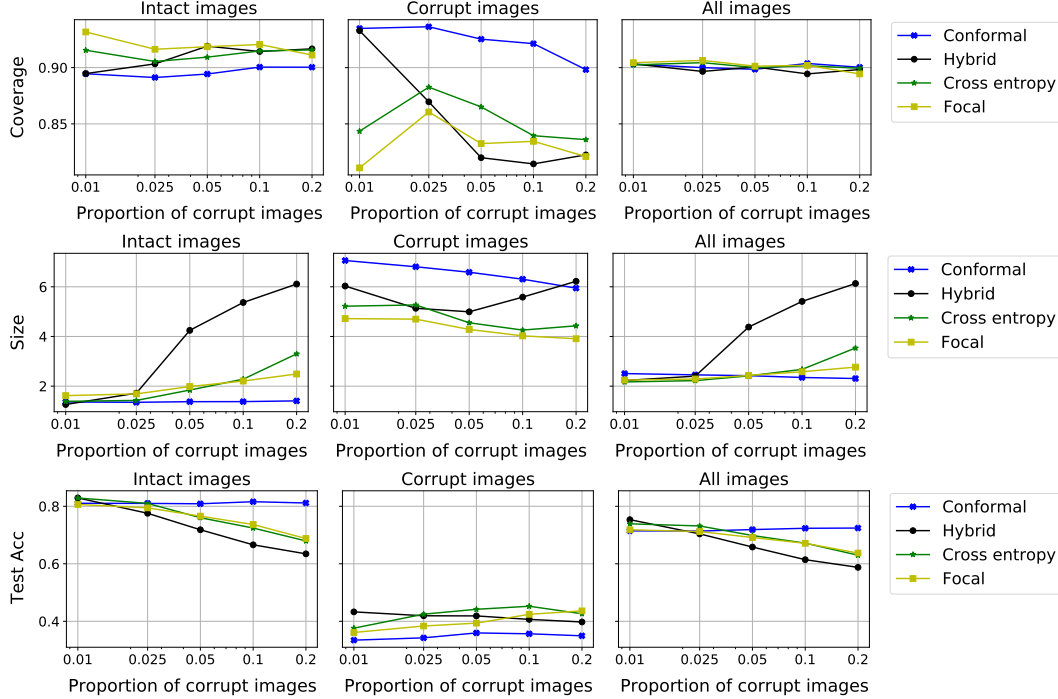


Figure A37: Performance of conformal prediction sets with 90% marginal coverage on CIFAR-10 data, based on convolutional neural networks trained with different loss functions. The results are shown as a function of the proportion of corrupt images in the training data. Top: conditional coverage, separately for intact and corrupt images. Middle: size of the prediction sets. Bottom: test accuracy. Other details are as in Figure A30.

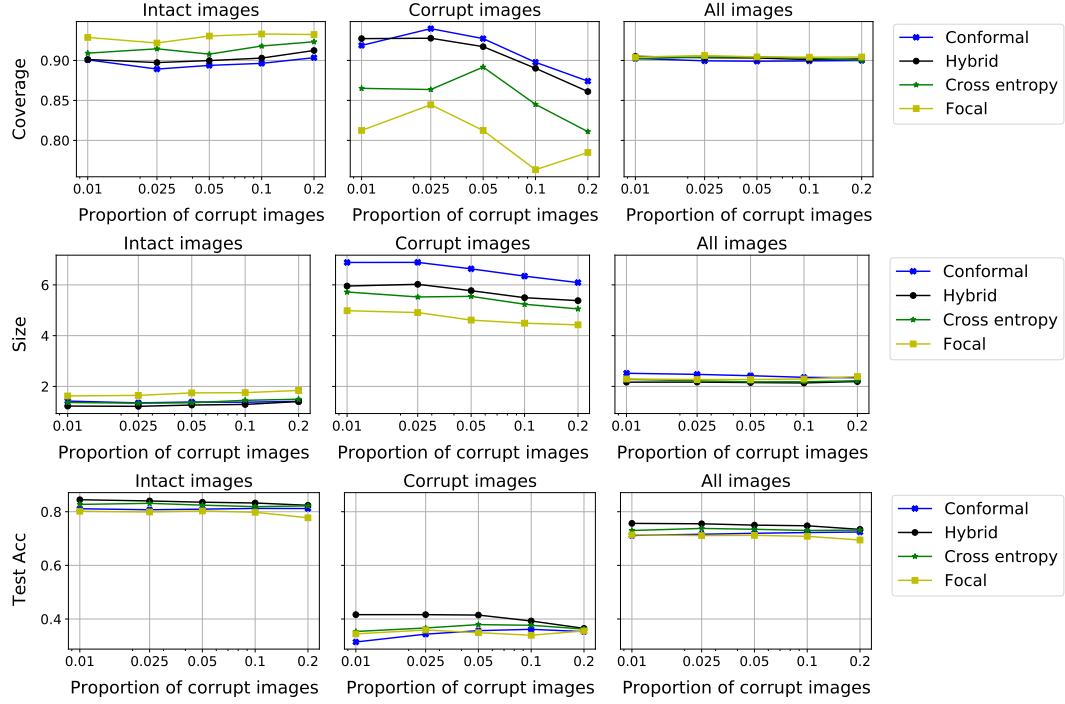


Figure A38: Performance of conformal prediction sets with 90% marginal coverage on CIFAR-10 data, based on convolutional neural networks trained with different loss functions. The models are trained with early stopping based on validation prediction accuracy. Other details are as in Figure A37.

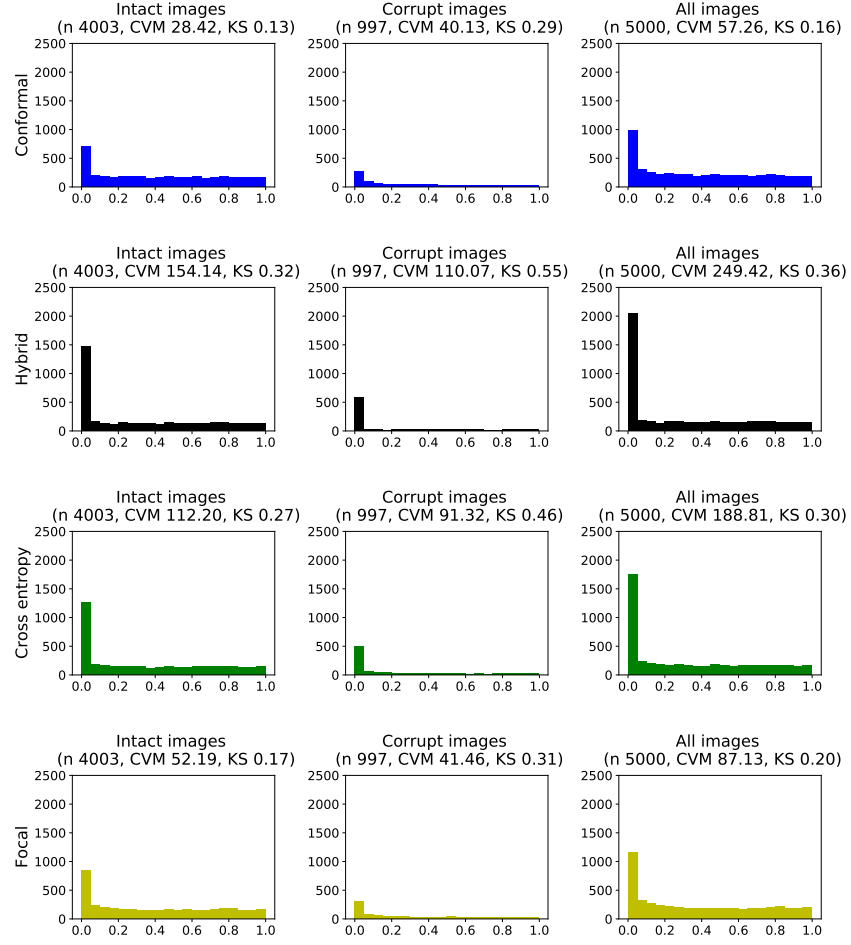


Figure A39: Histograms of conformity scores evaluated on test data and based on convolutional neural network models fully trained with different loss functions on 45000 images from CIFAR-10. The scores are reported separately for intact and corrupt images. The statistics in parenthesis at the top of each facet indicate the number of test samples, and the values of the Cramér-von Mises and Kolmogorov-Smirnov statistics for testing uniformity. Other details are as in Figure A30.

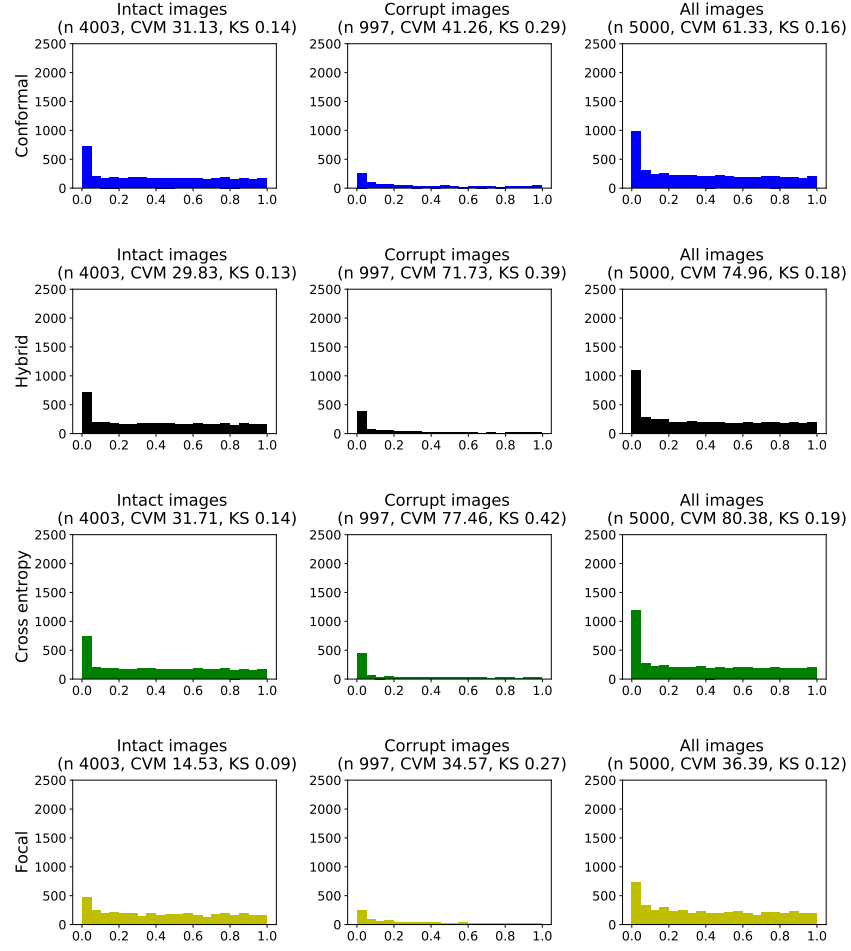


Figure A40: Histograms of conformity scores evaluated on test data and based on convolutional neural network models trained on 45000 images from CIFAR-10 with different loss functions and early stopping based on validation accuracy. Other details are as in Figure A39.

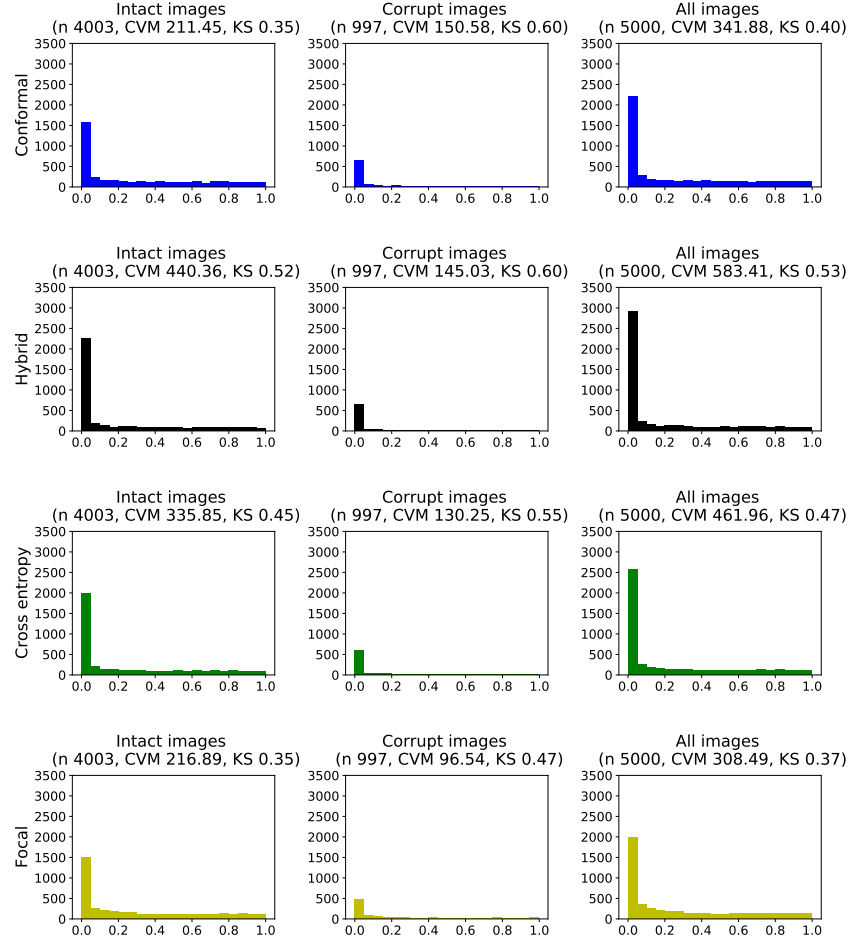


Figure A41: Histograms of conformity scores evaluated on test data and based on convolutional neural network models fully trained with different loss functions on 3000 images from CIFAR-10. Other details are as in Figure A39.

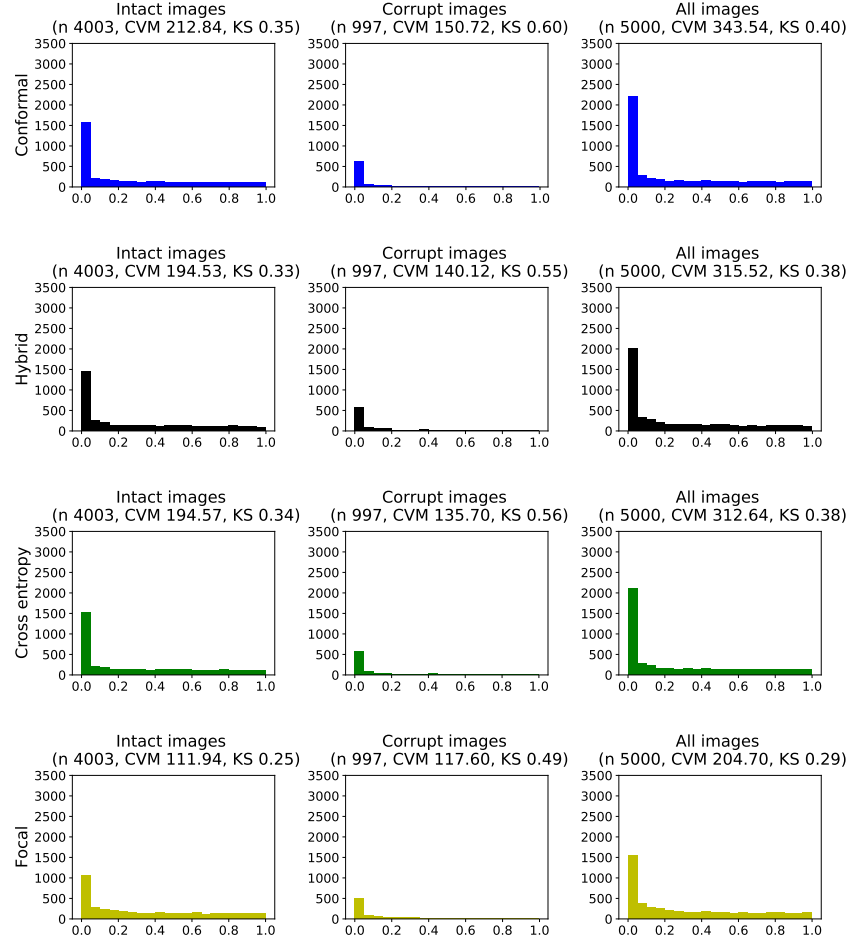


Figure A42: Histograms of conformity scores evaluated on test data and based on convolutional neural network models trained on 3000 images from CIFAR-10 with different loss functions and early stopping. Other details are as in Figure A40.

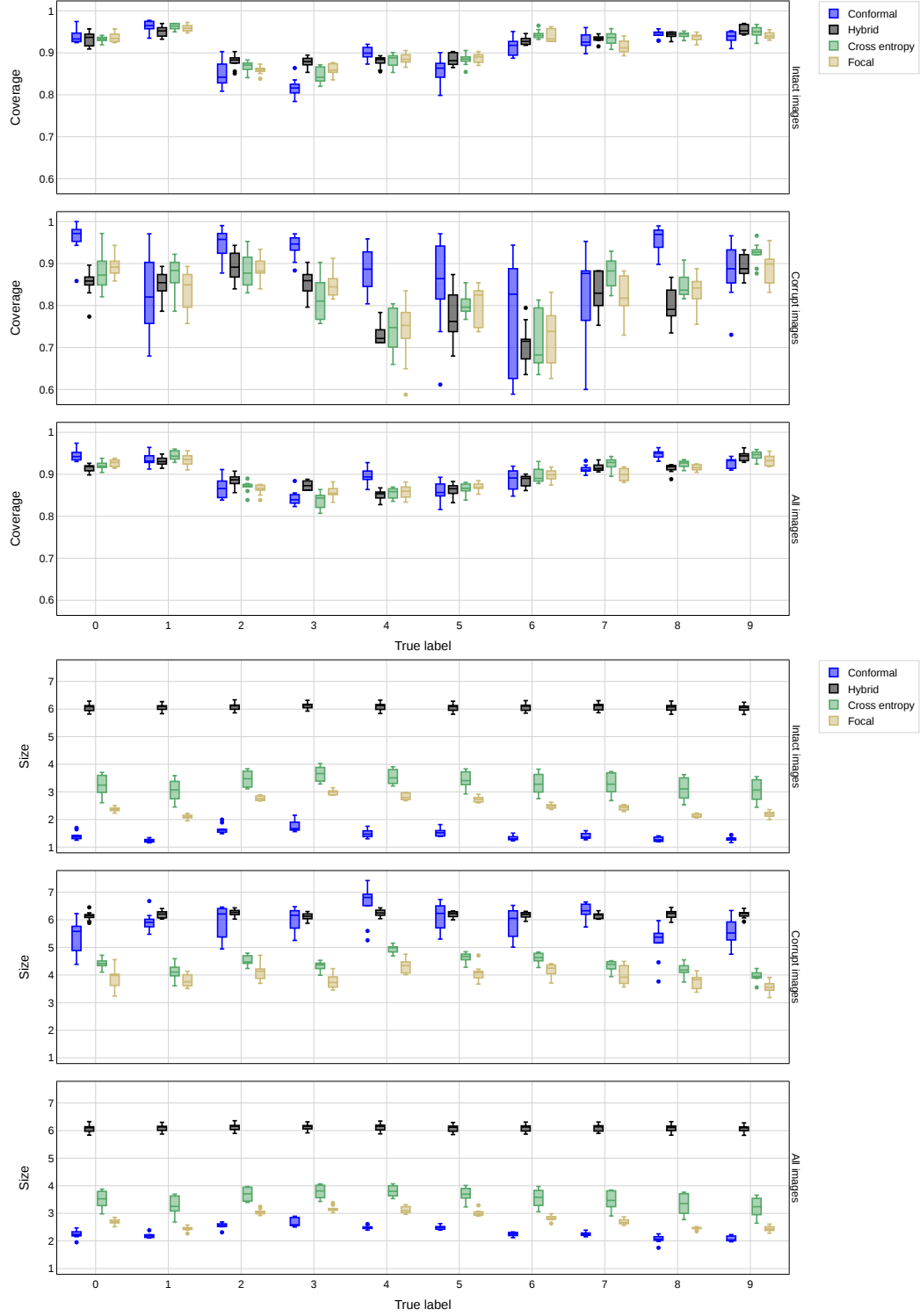


Figure A43: Coverage (top) and size (bottom) of conformal prediction sets with 90% marginal coverage on CIFAR-10 data, based on convolutional neural networks trained with different loss functions. The performance is reported separately for each true label. The models are fully trained on 45,000 images. Other details are as in Figure A30.

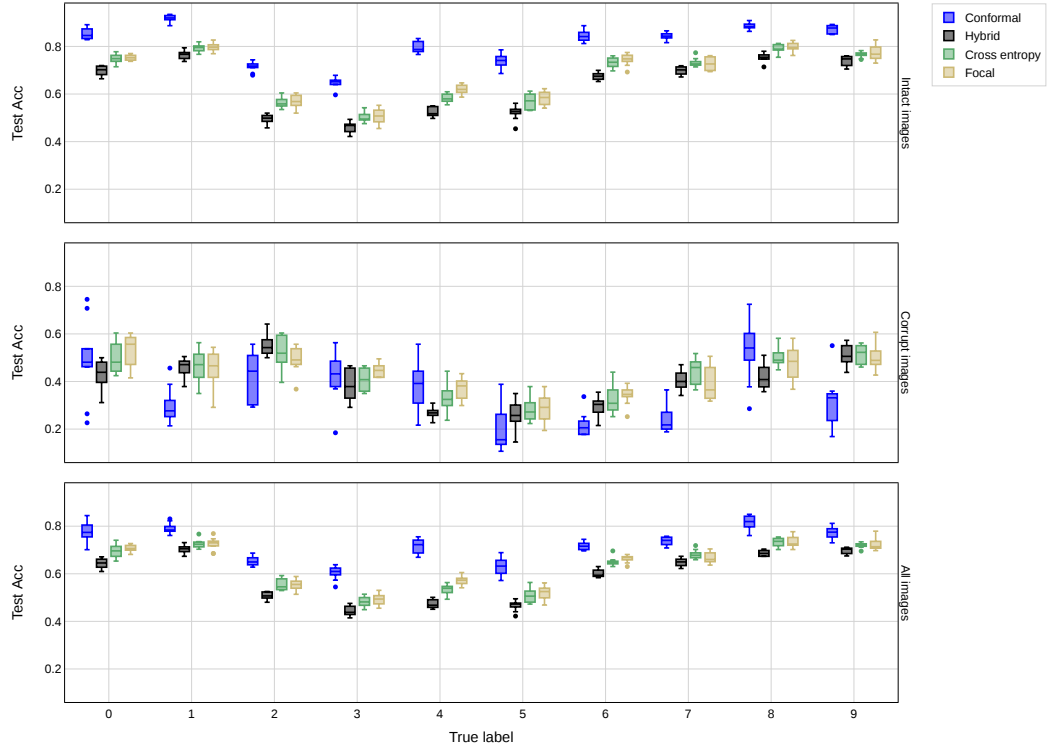


Figure A44: Test accuracy of convolutional neural networks trained with different loss functions. The performance is reported separately for each true label. The models are fully trained on 45,000 images. Other details are as in Figure A43.

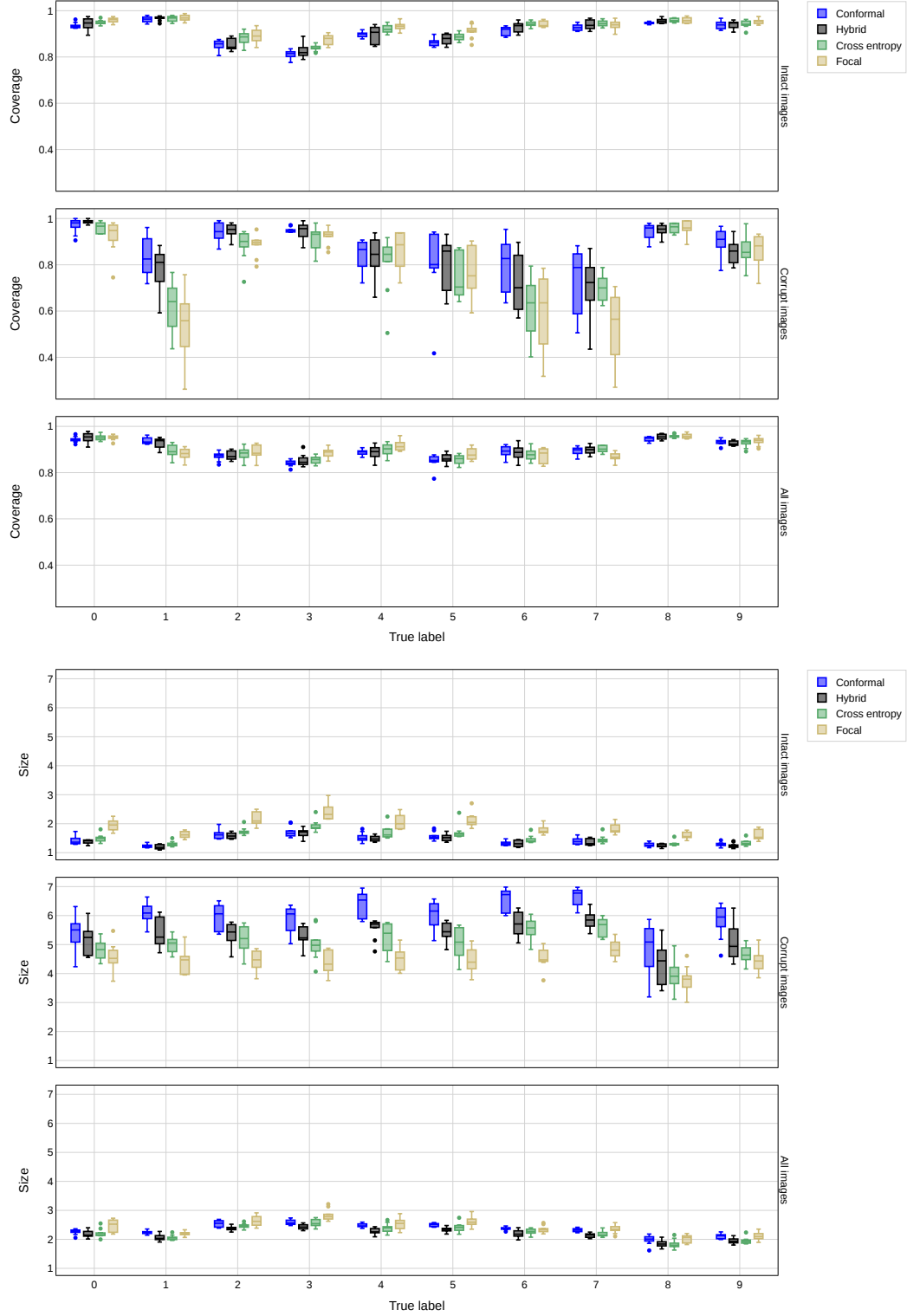


Figure A45: Coverage (top) and size (bottom) of conformal prediction sets with 90% marginal coverage on CIFAR-10 data, based on convolutional neural networks trained with different loss functions. The performance is reported separately for each true label. The models are trained on 45,000 images with early stopping based on validation accuracy. Other details are as in Figure A30.

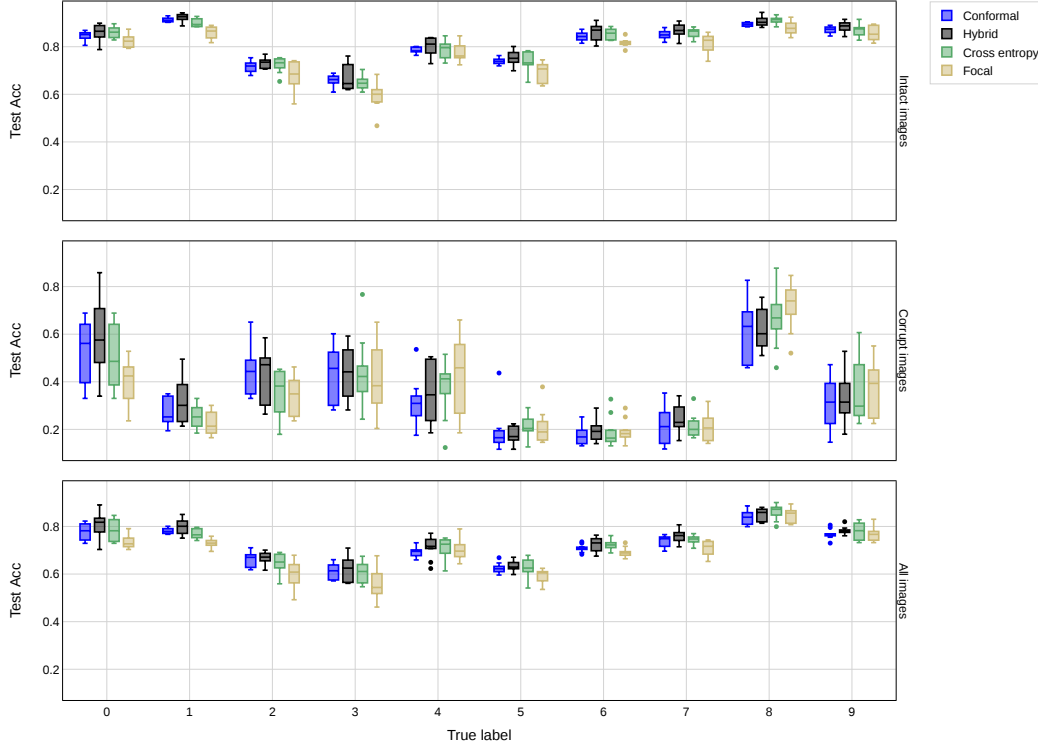


Figure A46: Test accuracy of convolutional neural networks trained with different loss functions. The performance is reported separately for each true label. The models are trained on 45,000 images with early stopping based on validation accuracy. Other details are as in Figure A45.

### A3.5 Details about experiments with credit card data

The models based on the conformal and hybrid losses are trained for 6000 and 4000 epochs, respectively, using the Adam optimizer with batch size of 2500. The initial learning rate of 0.0001 is decreased by a factor 10 halfway through training. The hyper-parameter  $\lambda$  controlling the relative weight of the cross entropy component is set equal to 0.1 for both losses. The models minimizing the cross entropy and focal loss are trained via Adam for 3000 epochs with batch size 500 and learning rate 0.0001, also decreased by a factor 10 halfway through training. These hyper-parameters were tuned to separately maximize the performance of each method.

### A3.6 Results with credit card data

	Coverage				Size all labels/0/1		Classification error		Distance from uniformity of conformity scores	
	Marginal		Conditional		Full	E.S.	Full	E.S.	Full	E.S.
	Full	E.S.	Full	E.S.						
Conformal	0.83	0.83	0.60	0.52	1.34/1.31/1.45	1.29/1.27/1.39	33.05	28.52	5.14/5.27/32.38	1.08/10.97/43.05
Hybrid	0.83	0.83	0.51	0.53	1.27/1.24/1.37	1.28/1.25/1.38	27.00	27.52	24.58/2.11/96.30	24.16/4.20/84.72
Cross Entropy	0.82	0.84	0.51	0.42	1.25/1.23/1.33	1.24/1.21/1.35	26.16	24.36	40.09/3.10/115.30	5.26/15.76/115.86
Focal	0.81	0.82	0.48	0.50	1.22/1.20/1.28	1.25/1.23/1.32	26.56	26.30	64.51/8.47/132.94	42.056/3.22/117.43

Table A5: Performance of conformal prediction sets with 80% marginal coverage on credit card default data, including also statistics measuring the distance from uniformity of the conformity scores evaluated on test data. Other details are as in Figure A5.

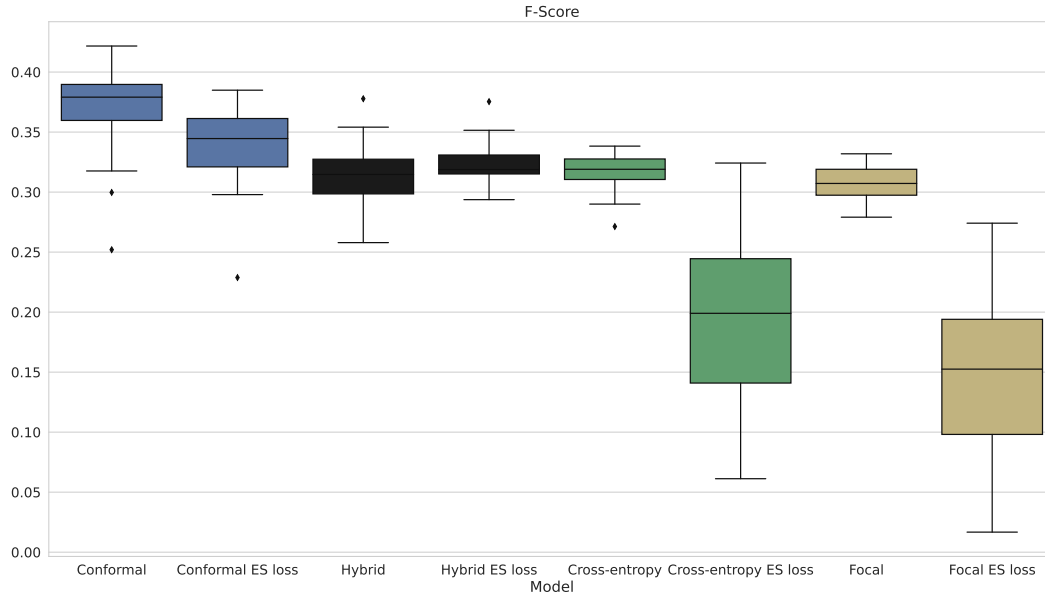


Figure A47: Empirical distribution over 20 independent experiments of the classification F-scores obtained with models trained with different methods on the credit card data set of Table 2.

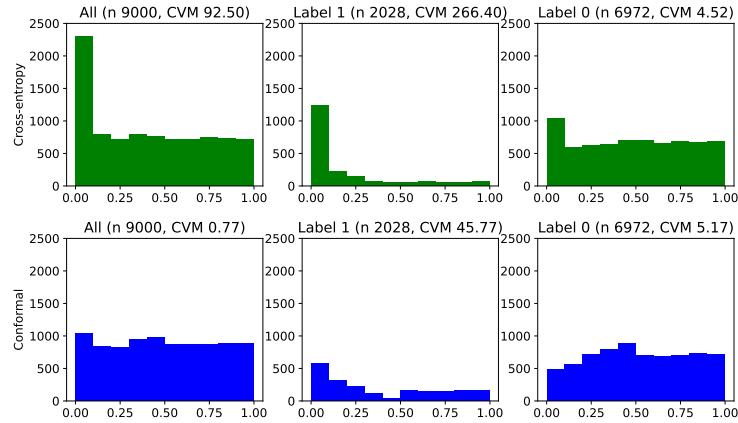


Figure A48: Histograms of conformity scores computed with models trained with different algorithms in simulations with credit card default data. The scores are evaluated on test data separately for samples with label 0 and 1. Top: Models trained with the cross entropy loss. Bottom: Models trained with the proposed conformal loss.